# Untangling differentiation in arc lavas: constraints from unusual minor and trace element variations at Salak Volcano, Indonesia

Heather K. Handley[a]*, Jon P. Davidson[a], Colin G. Macpherson[a], James A. Stimac[b]

[a]Department of Earth Sciences, Durham University, South Road, Durham, DH1 3LE, UK.

[b]Chevron Geothermal and Power, Sentral Senayan I, 11th Floor, Jalan Asia Afrika No. 8, Jakarta 10270, Indonesia.

*Corresponding author. hhandley@els.mq.edu.au

**Abstract**

Volcanic rocks from Salak Volcano in West Java display intriguing minor and trace element geochemical variations with silica. $TiO_2$ and $P_2O_5$ contents, Y, HFSE and REE concentrations are abnormally rich in the central vent group (CVG) lavas (e.g. Y = 32-69 ppm; Yb, 3-6.5 ppm) and display striking positive correlations with $SiO_2$. This contrasts with rocks erupted at side vents (SVG) on the eastern and western flanks of Salak and with rock suites of most other Javan volcanoes where these elements remain relatively constant with increasing $SiO_2$. Modelling of major and trace element data indicate that low pressure fractional crystallisation exerts strong control on the composition of CVG lavas. HFSE and HREE data are inconsistent with magma mixing, and can be explained by incompatible behaviour during fractionation of plagioclase, clinopyroxene and Fe-Ti oxide ± orthopyroxene and olivine. The observed variations in K/Rb and Ba/Th ratios and correlation of $^{87}Sr/^{86}Sr$ with indices of differentiation necessitate assimilation of a low K/Rb, low Ba/Th, Sr-rich contaminant with $^{87}Sr/^{86}Sr$ of ~ 0.7048 during fractional crystallisation. For the eastern flank SVG, deep fractionation of a phase in which HFSE and HREE are compatible (e.g. amphibole) is implicated. By extension, this is also suggested to occur beneath the majority of Javan volcanoes. Radiogenic isotope ratios (Sr-Hf-Nd) of Salak lavas are similar to other Javan lavas. SVG rocks erupted from the eastern flank vent have significantly more primitive Hf-Nd isotope ratios than other Salak volcanic rocks and may represent the least contaminated (by arc crust or subduction input) Salak lavas.

*Key words*: crustal contamination; fractional crystallisation; geochemistry; HFSE; petrogenesis; Sunda arc

## 1. Introduction

Understanding how geochemical signatures are imparted to arc rocks is problematic. Element compositions in arc lavas are dependent not only on the composition of the primary magma from which they originated, but also on the multitude of differentiation processes primary magma may suffer en route to the Earth's surface. Therefore elucidating composition-modifying processes in arc lavas is a prerequisite before the nature, composition and components of the source can be determined. Among the variety of processes capable of masking element concentrations of primary magmas, fractional crystallisation, crustal contamination and magma mixing (e.g. Ewart, 1982; Davidson et al., 1987; Hildreth and Moorbath, 1988; Tepley et al., 2000) are commonly identified in arc lavas.

Separate differentiation trends occur in lavas from within the single volcanic centre at Salak Volcano in West Java, and so this volcano provides a great opportunity to study the impact of shallow level processes on the composition of arc lavas. The steeply-sloped, positive correlations of HFSE (high field strength elements) and HREE (heavy rare earth elements) with indices of differentiation displayed by rocks erupted from the central vent at Salak are highly unusual compared to most other Sunda arc volcanic rock suites. This paper constrains the relative importance of various differentiation processes at Salak, in order to explain the abnormal HFSE-HREE differentiation trends displayed by the central vent eruptive products and their genetic relationship to flank vent volcanic rocks. This information is essential before the characteristics of the source can be investigated and it will aid in elucidating the nature of crust in West Java, of which relatively little is known. We suggest that fractionation of an (unseen) HFSE-HREE bearing phase plays an important role in the chemical evolution of most Javan island arc magmas.

## 2. Tectonic setting

Gunung Salak, 2211m, is a prominent stratovolcano located in the Quaternary volcanic front of the Sunda arc in West Java. The Sunda arc stretches from the Andaman Islands north of Sumatra to Flores in the Banda Sea and has developed as a result of the 6-7cm$^{-1}$ northward migration and consequent subduction of the Indo-Australian Plate beneath the Eurasian Plate (Le Pichon, 1968; DeMets et al., 1990; Tregoning et al., 1994). The tectonic features of the area have been described in detail by Hamilton (1979). Beneath Java (and Salak) the crust is ~20 km thick and has a 'quasi-continental' seismic velocity structure, intermediate between continental and oceanic (Ben-Avraham and Emery, 1973, Curray et al., 1977; Jarrard, 1986). Further east, seismic data indicate that the crust is ~18 km thick near Bali and 5-10 km beneath Flores (Curray et al., 1977). The south-eastern boundary of Sundaland (SE Asian continental part of the Sunda block/Eurasian plate with pre-Tertiary basement) is suggested by Hamilton (1979) to be located in West Java. However, due to limited knowledge of the precise structure and composition of the Javan crust, the exact location and nature of this boundary remain unknown.

## 3. Geology of Salak and sampling details

Salak forms the north-eastern part of the Salak-Perbakti-Gagak volcanic massif (Fig. 1), which consists of Upper Pleistocene to Recent stratovolcanoes, parasitic vents and phreatomagmatic craters. The Perbakti-Gagak range to the south-west is strongly eroded. Both areas in the north-east and south-west are sites of extensive hydrothermal activity. Intermittent volcanism occurred at Salak between ~0.2 to 1.2 my ago (Stimac, 2003). In historic time, volcanic activity at Salak has been limited to a number of phreatic explosions occurring at side vents on the flanks of the volcano. The summit area of Salak is characterised by two large breached craters, one open to the northeast and another to the southwest (Fig. 1), which are associated with volcanic sector collapse events. The westernmost crater was the

source of a large debris-avalanche deposit which extends over 10 km from the summit. Satellitic cones are mainly found on the south-west flank of Salak and on the northern foothills on the eastern side of the volcano. A late-stage dome built on the western crater rim is a result of the most recent activity.

The volcanic products of Salak can be divided into two main groups based on eruption location: those erupted from the central vent (CVG) and those erupted from flank or side vents (SVG). The CVG, consisting of multiple lava flows and pyroclastic units, dominates the volcanic deposits at Salak and therefore the majority of samples in this study were collected from this group (filled circles, Fig. 1). SVG samples S102 and S103 were taken from lava flows erupted from a side vent on the eastern slope of Salak. S107A and S107B SVG samples are from the western flank. Sampling of SVG products for geochemical analysis on the western flank was of limited success due to extensive alteration of lava caused by hydrothermal activity. Sample S112 is from a lava flow (SL3) thought to originate from the main vent (CVG) (Zaennudin et al., 1993). However, this sample is geochemically similar to the SVG samples in major and trace element composition. This unit extends down the western flank of Salak, therefore it is possible that S112 may have been erupted from one of the western side vents. As a result of uncertainty in the provenance of this sample it is distinguished from the other samples in all diagrams. Two pumice samples collected on the western slope of Salak (S100 and S101) are from extensive airfall deposits related to pre-Salak activity (Zaennudin, et al., 1993). These deposits are overlain by thinner airfall deposits from Salak. Limited dating has been carried out on Salak-Perbakti-Gagak volcanic products (Stimac, 2003). Reliance on geological maps and relative stratigraphy in this study limits a detailed temporal evaluation of Salak lavas and therefore this is not carried out here.

## 4. Analytical techniques

Mineral analyses were performed on carbon-coated polished slides of selected Salak volcanic rocks using a Cameca SX 100 at the University of Manchester NERC facility. The accelerating voltage was 15kV and beam current was 2nA. Detection limits (wt%) for Al, Mg, K, Ca, Ti are 0.01 or lower, Na, Si, Cr, Ni are around 0.03, while Fe is slightly higher around 0.08. Element precision is dependant on the mineral being analysed, but was typically less than 1% for Ca, Ti, Si, Al and Mg, between 1-2% for Fe, 2.7% for Ni and around 4% for Na, K, Mn and Cr.

Major element contents of Salak whole-rock samples were determined on fused glass discs produced by the Fusion method (spectroflux 105) using the Automated Philips PW2404 X-ray fluorescence spectrometer at the University of Edinburgh. In-house rock standards were used to calibrate the machine and monitor accuracy and precision during analysis.

Trace element concentrations of Salak rock powders were determined on the PerkinElmer ELAN 6000 quadrupole ICP-MS at Durham University following the analytical procedure and instrument operating conditions described by Ottley et al. (2003). Multiple analyses of procedural blanks (3 per batch), in-house standards and international reference materials: W2, BHVO-1, AGV1, BE-N and BIR1 during each session e.g. at the start, mid-way, and at the end of a run, allowed any drift in the instrument calibration to be detected. Reproducibility (internal and external) of standard values on the ELAN were less than 5% relative standard deviation.

Preparation of whole rock powders for Sr, Nd and Hf isotope analysis was undertaken in the Arthur Holmes Isotope Geology Laboratory (AHIGL) at Durham University. The sample dissolution procedure and chemical separation of Hf and Nd from rock samples is based on that presented by Dowall et al. (2003). The separation procedure for Sr follows that detailed by Charlier et al. (2006) except Sr was collect from the column in 300 µL MQ (rather than 0.05M $HNO_3$) followed by addition of 15 µL 10M $HNO_3$ to the collected Sr fraction. Sr, Nd

and Hf isotope ratios were determined on the AHIGL ThermoElectron Neptune Multi-collector Plasma Mass Spectrometer (MC-ICP-MS). Details of instrument operating conditions are presented in Nowell et al. (2003) and Dowall et al. (2003). Instrumental mass bias was corrected for using a $^{88}Sr/^{86}Sr$ ratio of 8.375209 (the reciprocal of the $^{86}Sr/^{88}Sr$ ratio of 0.1194), $^{146}Nd/^{145}Nd$ ratio of 2.079143 (equivalent to the more commonly used $^{146}Nd/^{144}Nd$ ratio of 0.7219) and $^{179}Hf/^{177}Hf$ ratio of 0.7325 plus an exponential law. Data quality was monitored over several analytical sessions by regular analysis of standard reference materials during each run. The reproducibility of the $^{87}Sr/^{86}Sr$, $^{143}Nd/^{144}Nd$ and $^{176}Hf/^{177}Hf$ ratios for the respective standard solutions in each of the individual analytical sessions are better than 21 ppm in all cases. Sr-Nd-Hf isotope data presented are plotted relative to NBS 987, J&M and JMC 475 standard values of 0.71024 (Thirlwall, 1991), 0.511110 (Royse et al., 1998) and 0.282160 (Nowell, et al., 1998) respectively. Blank samples processed (at least 2 per sample batch) were analysed by ICP-MS on the PerkinElmer ELAN 6000 quadrupole at Durham University. Total analytical blanks for Sr, Nd and Hf were below 1.2 ng for Sr (typically < 300 pg), 219 pg for Nd and 73 pg for Hf. These values are insignificant considering the quantity of Sr, Nd and Hf processed from the volcanic rocks (12-65 μg, 2-7 μg and 0.5-1.2 μg respectively).

Oxygen isotope analyses of mineral separates (~10mg per sample) were determined by laser-fluorination at Royal Holloway, University of London; using an analytical procedure following that of Macpherson et al. (2000). In-house standard values of SC olivine 2 and GMG II during the period of study were within 0.01‰ of accepted values: +5.24‰ ± 0.04 (1σ, n = 6) and +5.69‰ ± 0.08 (1σ, n = 15), respectively. Oxygen yields were slightly low, but consistent over the individual sessions: 93% for plagioclase (n = 7) and between 92-94% (n = 20) for clinopyroxene. Replicate analyses of plagioclase and clinopyroxene throughout

the study were within 0.09‰ and 0.04‰ respectively. Oxygen results are reported as per mille deviations relative to the standard mean ocean water (V-SMOW) standard.

## 5. Petrology and mineral chemistry

Modal analyses of Salak lavas and representative mineral compositions are given in Tables 1 and 2-5, respectively. Andesites are the most common rock type sampled at Salak. The andesites of the SVG are generally more phenocryst rich than those of the CVG with total phenocryst abundances ranging between ~50-60 % and 20-46 % (modal volume), respectively (Table 1). Both andesite groups contain a typically observed island-arc mineral assemblage of plagioclase, clinopyroxene, orthopyroxene and Fe-Ti oxide. Basaltic-andesites of the CVG contain olivine phenocrysts, which commonly occur with both clinopyroxene and orthopyroxene (indicating magmatic disequilibrium in the latter case). The olivine phenocrysts ($Fo_{54-66}$, Table 2) are generally small and subhedral, some showing slight alteration to iddingsite at crystal edges. The SVG rhyolite and Pre-Salak pumice samples are dominated by glassy groundmass and phenocrysts of plagioclase with minor pyroxene. Small amounts of amphibole and quartz ± biotite are also present (Table 1).

Orthopyroxene phenocrysts in the basaltic-andesites of the CVG are mostly subhedral-euhedral and infrequently contain smaller inclusions of early-formed olivine (S104). In some basaltic-andesites (S104, S105 and S108) the orthopyroxene phenocrysts are surrounded by a thin rim, or jacket of clinopyroxene. This disequilibrium feature appears to be relatively common in arc lavas and has been observed in the volcanic products of several Javan volcanoes: Ijen (Sitorus, 1990), Slamet (Vukadinovic and Sutawidjaja, 1995), Lamongan (Carn and Pyle, 2001) and Gede (Handley, 2006). Mineralogically, clinopyroxene and orthopyroxene in the basaltic andesites of the CVG lack evidence for compositional disequilibrium, displaying normal zoning of phenocrysts from Mg-rich cores towards more

Fe-rich rims. Orthopyroxene and clinopyroxene compositions available for the andesites show slightly more variation in the SVG than the CVG (Figs. 2a & b). The limited pyroxene analyses available for the SL3 lava show restricted compositional variation (Fig. 2c).

Plagioclase is the most abundant phenocryst phase in all CVG and SVG rocks. Plagioclase phenocrysts exhibit a wide range in composition in the basaltic-andesites of the CVG (Figs. 3a & b; Table 4), with plagioclase rims displaying the largest variation in anorthite content ($An_{58-91}$). Phenocryst interiors are more restricted in composition and have fairly high An contents (above 80). The An contents of several plagioclase rims are higher than those in respective groundmass plagioclase (< $An_{55}$) indicating that not all phenocrysts were in equilibrium with the host liquid. Disequilibrium textures of plagioclase phenocrysts (oscillatory zoning, sieve textures and infrequent resorbed cores) are observed in all CVG basaltic-andesite samples. CVG and SVG andesites display similar compositional ranges in plagioclase (Table 4). In the CVG (Fig. 3c) plagioclase phenocryst and groundmass compositions are extremely homogeneous ($An_{48-59}$) with the exception of one core analysis ($An_{72}$). The SVG plagioclases display a slightly wider compositional range and often the core sections possess lower anorthite contents than respective mid and rim sections (Fig. 3e). Sieve textures and oscillatory zoning are common in plagioclase phenocrysts of both groups of andesites. The SL3 andesite displays a fairly restricted range in plagioclase composition ($An_{54-68}$) similar to the andesite analysed from the CVG (Fig. 3d). Some SL3 plagioclase phenocrysts show reverse zoning from less An-rich cores to more An-rich rims.

Fe-Ti oxide (titanomagnetite) occurs as a phenocryst phase in all rocks and is often associated with the other mafic phases, commonly occurring as inclusions within pyroxene, or forming a glomerocrystic texture with pyroxene. Titanomagnetite is slightly more Ti-rich in the CVG andesite compared to the SVG andesite (Table 5).

Cognate xenoliths are observed in SVG samples from the eastern flank unit, PD1 (S102 and S103), displaying sharp contacts with the surrounding lava. The xenoliths are composed of heavily sieve-textured and oscillatory-zoned plagioclase phenocrysts, clinopyroxene, orthopyroxene and Fe-Ti oxide phenocrysts (titanomagnetite and ilmenite; in close association with ferromagnesian minerals) set in a medium-grained groundmass. The groundmass is dominated by euhedral plagioclase laths, elongate acicular pyroxene, small oxide crystals and minor devitrified glass. Clinopyroxene occasionally forms thick jackets around orthopyroxene phenocrysts. Fig. 2b shows there is some overlap in clinopyroxene and orthopyroxene compositions between the xenolith (black crosses) and the host rock (open squares). However, orthopyroxene phenocrysts in the xenolith also contain significantly more En-rich compositions. Plagioclase compositions in the xenolith (Fig. 3f) are scattered, but generally more An-rich than those in the host lava (Fig. 3e).

## 6. Geochemistry

### *6.1. Major and trace element variations*

Major and trace element data are reported in Table 6. Salak lavas are relatively evolved, with MgO contents less than 4 wt %. Salak volcanic rocks display negative correlations on diagrams of $Al_2O_3$, $Fe_2O_3$, MgO and CaO against $SiO_2$, and positive correlations between $SiO_2$ and both $K_2O$ and $Na_2O$ (Fig. 4), although $Na_2O$ contents in the SVG are relatively constant with increasing $SiO_2$. $TiO_2$ and $P_2O_5$ variation is split into two markedly different trends. Lavas erupted from the CVG generally show an increase in $TiO_2$ and $P_2O_5$ contents with increasing $SiO_2$, whereas SVG lavas possess lower $TiO_2$ and $P_2O_5$ contents and plot within the field of other Javan volcanic rocks (Figs. 4g and h). $TiO_2$ and $P_2O_5$ contents measured in the more evolved CVG rocks (~60% $SiO_2$) are unusually high (up to 1.18 and 0.48 wt%, respectively) when compared to the majority of values reported for other Javan

lavas (Fig. 4g) and from volcanic rocks of other island arc systems at comparable silica content e.g. Kermadec (Gamble et al., 1993; Ewart et al., 1994; Turner et al., 1997), Lesser Antilles (Thirlwall et al., 1996; Zellmer et al., 2003) and Mariana (Woodhead, 1989; Elliot et al., 1997). Increasing $TiO_2$ content with increasing silica (Fig. 4g) is not normally observed in arc andesites, most probably due to the early fractionation of magnetite (Gill, 1981; Pearce, 1982).

The high field strength elements (HFSE) and the rare earth elements (REE), particularly the heavy REE, also show abnormally high concentrations in the more evolved CVG samples (Y = 32-69 ppm; Yb, 3-6.5 ppm) and display strikingly positively-sloped, linear trends on $SiO_2$ variation diagrams (Figs. 5a and b). This contrasts again with the SVG rocks and the majority of other volcanic rock suites of Java, where concentrations remain relatively constant with increasing $SiO_2$ (Figs. 5a and b). High concentrations of $TiO_2$, $P_2O_5$, Y and systematic increases of these elements with $SiO_2$ are so far only evident at one other volcano in Java, namely Tengger Caldera in East Java (Figs. 4g and h and 5a). This unusual feature was not noted in the study of Tengger Caldera by van Gerven and Pichler (1995). Extensive comparisons of trace element variations between Tengger Caldera and Salak are however restricted due to the limited geochemical data available for the former volcanic system. In contrast to the separate HSFE and REE variation trends displayed by the CVG and SVG, variations in large ion lithophile elements (LILE) are similar, displaying positive correlations with $SiO_2$ (Figs. 5e and f). Sr generally decreases as $SiO_2$ increases within each group (Fig. 5g). The SVG rocks containing around 60 wt% $SiO_2$ are slightly displaced below the main Salak trend in the majority of these diagrams with the exception of Sr, where they sit at slightly elevated values.

Chondrite normalised REE patterns of selected Salak lavas are displayed in Fig. 6. Salak volcanic rocks are enriched in the light REE compared to mid-ocean ridge basalts (Normal-

MORB and Indian Ocean-MORB). With the exception of the high silica rhyolite, the heavier REE show concentrations more similar to those in MORB than the light REE. The higher silica CVG andesite is located parallel to, but at higher REE concentrations than the less evolved CVG rock. The enrichment of the REE in the evolved CVG sample is made clear when compared to a SVG rock of comparable silica content (unfilled squares). Strong depletions are observed in the middle to heavy REE concentrations of the high $SiO_2$ (west flank) SVG rocks, compared to less evolved Salak rocks.

*6.2. Radiogenic isotopes*

Sr, Nd and Hf isotope data are presented in Table 6 and shown in Figs. 7 and 8. $^{87}Sr/^{86}Sr$ and $^{143}Nd/^{144}Nd$ isotope ratios of Salak volcanic rocks define a negative array, lying within the field of previously published Java data. Salak exhibits a relatively wide range in $^{87}Sr/^{86}Sr$ ratios, 0.704262 to 0.705051, although the majority of the lavas are more tightly constrained within the range 0.704569-0.705051. The two SVG samples, S102 and S103, erupted on the eastern flank of Salak are displaced from the rest of the Salak lavas, possessing significantly lower $^{87}Sr/^{86}Sr$ and higher $^{143}Nd/^{144}Nd$ ratios (Fig. 7 inset). In Hf-Nd isotope space (Fig. 8), Salak volcanic rocks also lie within the field defined by Java, possessing lower $^{143}Nd/^{144}Nd$ and $^{176}Hf/^{177}Hf$ isotope ratios than MORB, and higher ratios than Indian Ocean sediments. The eastern-flank SVG samples, S102 and S103, possess significantly more primitive $^{176}Hf/^{177}Hf$ isotope ratios compared to the other Salak lavas (Fig. 8 inset).

*6.3. Stable isotope data*

Oxygen isotope data from mineral separates are presented in Table 7. The restricted clinopyroxene and plagioclase analyses of Salak lavas have low $\delta^{18}O$ values ranging from +5.18 to +5.44‰ (n = 3) and +5.96 to +6.07‰ (n = 4), respectively. The former values are

similar to mantle clinopyroxene $\delta^{18}O$ values reported by Mattey et al. (1994) and Ionov et al. (1994): +5.57 ± 0.32‰ and similar to or slightly lower than those reported from other volcanoes in Java (Galunggung, Harmon and Gerbe, 1992; Gede Volcanic Complex, Handley, 2006; Ijen Volcanic Complex, Handley et al., 2007). Plagioclase $\delta^{18}O$ values of Salak are generally higher than those of Galunggung (+5.6 to +6.0‰, Harmon and Gerbe, 1992), but lower than those analysed in Merapi volcanics (+6.5 to +7.00‰, Gertisser and Keller, 2003a). Differences in $\delta^{18}O$ values between coexisting plagioclase and clinopyroxene ($\Delta_{plag\text{-}cpx}$) are between 0.63 to 0.79‰ and suggest most of the mineral pairs record oxygen isotopic equilibrium at typical magmatic temperatures for andesite liquids. The limited number of analyses from Salak prohibits intra-group comparisons of $\delta^{18}O$ data, however, the lowest $\delta^{18}O$ clinopyroxene value is measured in the sample with the most primitive radiogenic isotope ratios (SVG, S103).

## 7. Discussion

Minor and trace element variations at Salak are intriguing, and raise two important questions: 1) Why do the CVG display atypical differentiation trends and unusually high concentrations in minor and trace elements, in particular for the HREE, Y, $TiO_2$ and $P_2O_5$ compared to other Javan volcanoes? 2) Why are there strikingly different differentiation trends in lavas from a single volcanic centre?

Assuming that variations in the silica content of volcanic rocks are generated as a result of differentiation of magma (Gill, 1981; Davidson et al., 2005), systematic increases of Y, Yb, $TiO_2$ and $P_2O_5$ with $SiO_2$ within the CVG (Figs. 5a & b and Figs. 4g & h, respectively) are compelling evidence for geochemical variation being imparted during differentiation in the crust e.g. through magma mixing, fractional crystallisation and/or combined assimilation and fractional crystallisation.

*7.1. Differentiation in the Central Vent Group*

*7.1.1. Magma Mixing*

Magma mixing is identified as an important composition-modifying process within the evolution of many arc magmas (e.g. Conrad et al., 1983; Tepley et al., 2000) including some Sunda arc magmas (Slamet, Reubi et al., 2002; Merapi, Gertisser and Keller, 2003b; Batur, Reubi and Nicholls, 2004). Linear correlations displayed by the CVG rocks on bivariate element-silica diagrams (Figs. 4 and 5) suggest that chemical variation within this group may be explained by the interaction and mixing of chemically distinct magmas. Phenocryst textures and mineral disequilibria in CVG lavas (section 5) indicate that open system processes may have occurred at one or several points in the magmatic evolution of the CVG.

A purely geochemical approach to evaluate mixing processes utilises element ratios (Langmuir et al., 1978; Vogel, 1982; Flood et al., 1989). Magma mixing should produce hyperbolic arrays in plots of a trace element ratio versus a concentration. Figs. 9a and b show that the CVG data largely define a curved array on some element-ratio diagrams. K/Rb and Ba/Th ratios were chosen as these ratios correlate with $SiO_2$ and display a wide range in the CVG. The former ratio is also a potentially useful monitor of crust-magma interaction (Davidson, 1987, Hildreth & Moorbath, 1988), providing that the melt and crust have distinctive values for the ratio. K/Rb and Ba/Th ratios are plotted against Rb (which represents the degree of magmatic differentiation) and Yb (to check whether the model can account for the highly unusual variations in concentrations observed for this element). The results of bulk-mixing calculations between one of the least evolved CVG samples (S106B) and several end members are shown in Figs. 9a and b. If element variation in the CVG is a result of simple mixing, the other end member must be more evolved (higher $SiO_2$) in composition. Granite xenoliths found within a deposit of cream tuff in the Perbakti-Gagak

area adjacent to Salak provide evidence for the presence of evolved, granitic material (Stimac, 2003) in West Java. No data are available from this granite for use in modelling, therefore the more evolved end member magmas in mixing calculations are represented by a rhyolite from Salak (S107A) and by arc-related granites from some of the southern-most plutonics in Sumatra (i.e. close to West Java): monzodiorite (75413) and granodiorite (75415) (Gasparon, 1993). Mixing with a more basic end member (tholeiitic lava) from Guntur in West Java (Edwards, 1990) is also shown for comparison. The end member compositions used in mixing calculations are given in Table 8.

Fig. 9a shows that mixing in K/Rb-Rb space between S106B and a granitic sample with a high K/Rb ratio (MM D) is unable to generate a mixing curve to fit the CVG data. Similar unsatisfactory mixing trends would result from mixing with bulk upper-crustal material, which also has relatively high K/Rb (~250; Taylor, 1977). Mixing between S106B and granodiorite (MM B) or Javan tholeiite (MM C) also fail to fit the data, generating curves that have a large decrease and increase (respectively) in K/Rb ratio, with only a small change in Rb. The mixing curve produced using the Salak rhyolite (MM A) as the evolved end member, produces the best fit to the CVG data. Fig. 9b, Ba/Th-Yb, shows mixing curves generated between the same end members in Fig. 9a. Mixing in all cases is inadequate in explaining the Salak CVG data due to the low Yb content of the end members chosen. Low Yb contents of basic and evolved Javan lavas and evolved Sumatran plutonics, suggests that Yb contents of the CVG cannot be explained by simple mixing.

*7.1.2. Fractional crystallisation*

Fractional crystallisation was modelled by least squares analysis of Salak major element data using the XLFRAC programme (Stormer and Nicholls, 1978; Table 9). The results suggest that the most evolved CVG lava can be produced by fractionation of the least evolved

CVG lava by 61% crystallisation ($\Sigma r^2 = 0.13$; model 1). Smaller values of $\Sigma r^2$ are obtained in models to less differentiated final lavas (models 2 & 3), regardless of whether orthopyroxene or olivine is included in the mineral assemblage (compare models 3 & 4). This suggests that major and minor element variation within the CVG can be explained by fractional crystallisation of plagioclase, clinopyroxene, Fe-Ti oxide +/- olivine and orthopyroxene (e.g. Figs. 4g and h). But, can fractional crystallisation explain the unusual trace element variation trends not seen in the majority of Javan lavas using the same mineral assemblage?

Y and the REE often behave as incompatible elements in primitive arc tholeiites, however they usually remain constant or decrease in concentration with increasing magmatic fractionation in the calc-alkaline series, where they can be accommodated within amphibole, apatite and zircon (Pearce, 1982). This is exemplified by the Java data in Figs. 4g and h, and amphibole fractionation curves in Figs. 5a and b. To examine whether fractional crystallisation can produce the large increases in Y, Yb and Ti of the CVG (over a relatively narrow range in silica) and test the conclusions of least squares analysis, simple calculations were made using the Rayleigh fractionation equation: $C_l = C_o F^{(D-1)}$ where $C_l$ is the concentration of an element in the liquid, $C_o$ is the concentration of an element in the original liquid, $F$ is the fraction of liquid remaining and $D$ is the bulk distribution coefficient. The degree of fractionation ($F$) and the phase proportions used are those suggested by major element modelling (Table 9, model 1). The distribution coefficients used are given in Table 10. Calculated Ti, Y and Yb compositions expected in the daughter rocks (Table 10, Figs. 4g, 5a and b) show that incompatible behaviour of HFSE and HREE during fractional crystallisation can account for the high concentrations of these elements in Salak rocks. In all three models in Table 10 the concentrations predicted in the daughter rocks are higher than those actually measured. This contrasts with the results of mixing (Fig. 9b) between a basic CVG rock and the tholeiitic and more evolved volcanic and plutonic samples, which were

unsuccessful in accounting for high Yb concentrations. Fractional crystallisation curves (FC) are shown on K/Rb-Rb and Ba/Th-Yb diagrams (Figs. 9a and b) for removal of the same mineral assemblage used above. It should be noted that an identical FC curve is produced if the modal mineral assemblage of S106B (Table 1) is used instead. The Salak CVG data diverge from the calculated FC curve towards lower K/Rb and Ba/Th, thus suggesting that pure closed-system fractional crystallisation cannot explain all of the geochemical variation observed in the CVG lavas.

### *7.1.3. Assimilation and Fractional Crystallisation (AFC)*

AFC processes are recognised in the evolution of magma in arc settings (Davidson et al., 1987; Hildreth and Moorbath, 1988; Davidson and Harmon, 1989) and have been suggested for the Sunda arc (Gasparon et al., 1994). Little is known about the nature and composition of the crust in West Java. Seismic velocities suggest that the crust in West Java is thicker than that at the eastern end of Java (Ben-Avraham and Emery, 1973; Curray et al., 1977; Kieckhefer et al., 1980) and in West Java the arc may be built on continental material, i.e. Sundaland pre-Tertiary basement (Hamilton, 1979). Large granite blocks found in a tuff deposit in the vicinity of Salak (Perbakti-Gagak area, Fig. 1) display partially melted margins with adhering rhyolitic lava (Stimac, 2003). It is unknown when this granite was emplaced in the crust, but it suggests that interaction and possible contamination of magma by evolved plutonic rocks may occur at Salak. AFC curves are shown on Figs. 9a and b for contamination of the most basic Salak magma, by evolved volcanic (AFC A) and plutonic (AFC B) rocks, possessing low K/Rb and Ba/Th ratios. These curves fit the array of Salak data well, even though the contaminants possess low Yb concentrations (cf. mixing) Assimilation of upper and bulk crust (e.g. Taylor, 1977; Sumatran granitoid 75413) would generate concave-down AFC curves, inconsistent with the CVG data. It was suggested by Hamilton (1979) that the

crust in West Java is not truly silicic in character and may consist of older volcanic-arc rocks and ophiolite slivers. However, AFC models involving basic arc rocks (e.g. Fig. 9 AFC C) and a range of basic and ophiolite compositions (see below) are also inconsistent with the CVG array.

In summary, major and trace element modelling suggests that the unusual increases in HFSE and HREE with increasing $SiO_2$ are created due to incompatible behaviour of these elements during fractional crystallisation. Systematic variations in some trace element ratios (K/Rb and Ba/Th) and disequilibrium textures observed in the rocks indicate that assimilation of a contaminant with low K/Rb and Ba/Th ratios occurs during fractional crystallisation in the crust.

***7.1.4. Isotopic constraints***

Continental-type crustal rocks commonly have elevated $^{87}Sr/^{86}Sr$ isotope ratios compared to Quaternary volcanic rocks and mantle-derived magmas. Assimilation of crust during crystal fractionation (DePaolo, 1981) in arc magmas may therefore cause modification to the isotope ratios in resultant lavas. Consequently, a plot of Sr isotope ratio against an index of differentiation, e.g. $SiO_2$, can be used to detect AFC processes, in cases where the crust being assimilated is isotopically distinct. Even though the number of samples with isotope data is relatively limited and the variation in $^{87}Sr/^{86}Sr$ of the CVG is small, the more evolved CVG samples display generally higher $^{87}Sr/^{86}Sr$ ratios (Fig. 10), and the data patterns observed in this plot are identical (though the inverse) to those of Ba/Th with $SiO_2$ (see inset to Fig. 10). This suggests that Ba/Th, for which there is more data compared to $^{87}Sr/^{86}Sr$, might serve as a proxy for isotopic composition. The roughly hyperbolic trend observed in Fig. 10 and variation in $^{87}Sr/^{86}Sr$ isotope ratio with $SiO_2$ in the CVG further support control by differentiation, and more specifically by AFC processes.

The five CVG data points define a concave-down hyperbola on Ba/Th versus $^{87}Sr/^{86}Sr$ (Fig. 11). The AFC curves displayed here are for the same AFC end members used in trace element modelling (see Fig. 9 caption for details). Neither model on Fig. 11 using evolved volcanic nor plutonic rocks produces hyperbolic curves to fit the CVG data. AFC curves for these models largely follow the same vertical trend shown by fractionation crystallisation (FC) alone (arrow, Fig. 11), and altering the rate ratio of mass assimilated to mass crystallised (*r*) has little effect on the shape of the curve. The basic contaminant (see captions to Figs. 9 and 10 for details) produces an AFC curve (C) with a much better fit to the CVG data, but suggests a large amount of contamination is required compared to crystallisation ($r = 0.8$). Such high AFC *r*-values are not unreasonable and have been proposed for differentiation of basalts at Jebel Marra volcano in Sudan (Davidson and Wilson, 1989) and by Bourdon et al. (1998) for the Grande Comore volcanics.

A contaminant with a significantly higher Sr content than that of the parental rock would be able to generate a hyperbola curving in the required direction from the parental composition of S106B and not necessitate such a high r-value. Fig. 10 also indicates this as assimilation of a contaminant with low Sr concentration would produce a concave-up curve initially projecting in a horizontal direction away from the least evolved CVG sample, which is inconsistent with the concave-down data array in Fig. 10. The apparent plateau in $^{87}Sr/^{86}Sr$ isotope ratio in $SiO_2$-rich CVG rocks suggests that the $^{87}Sr/^{86}Sr$ ratio of the contaminant is asymptotic to the $^{87}Sr/^{86}Sr$ ratio of the more evolved CVG samples (i.e. ~0.7048). If the distribution coefficient for Sr in plagioclase is greater than one, then a magma crystallising this phase would become progressively more sensitive to Sr in the contaminant (which is assumed to be fixed). The more AFC magma endures, the more isotopically sensitive to the contaminant it would become, and therefore, for a given shift in silica the magma would obtain a larger shift in $^{87}Sr/^{86}Sr$ isotope ratio if the contaminant had a higher $^{87}Sr/^{86}Sr$ ratio.

Consequently, it is argued that if the data are consistent with AFC, the contaminant has a high Sr concentration and Sr-isotope ratio ~0.7048 (curved arrow, Fig. 10) contamination by a high $^{87}Sr/^{86}Sr$ component would result in a data array with a steeper positive correlation on Fig. 10 (diagonal arrow). The moderate decrease in Sr concentration with increasing $SiO_2$ in the CVG (despite the modelled involvement of large amounts of plagioclase fractionation) further argues for a high-Sr assimilant. An AFC calculation using S106B as the parent magma and the Sumatran granodiorite as the contaminant suggest that to produce a concave-down hyperbola to fit the data in Fig. 11 an extremely unrealistic Sr concentration in the contaminant of >7000 ppm is required. Evolved volcanic or plutonic contaminant end members are unlikely to possess higher Sr concentrations than the basaltic andesite S106B being contaminated as Sr content generally decreases with differentiation in arc-related igneous rocks due to plagioclase fractionation. Incorporation of the assimilant as a partial melt (0.1 - 10% melting), rather than bulk addition of this component, does not increase the Sr concentration sufficiently enough to improve the fit of the models for Ba/Th versus Sr isotope ratio and also leads to a more rapid decrease in Ba/Th ratio, creating an AFC trend further away from the CVG array.

If Sr isotope variation in the CVG is controlled by AFC processes as suggested above, then the contaminant is characterised by high Sr concentration, $^{87}Sr/^{86}Sr$ isotope ratio of around 0.7048 and low K/Rb and Ba/Th ratios (< ~110 and < ~45, respectively). Table 11 shows trace element data and Sr-isotope ratios for a variety of rocks that may represent the West Javan crust and could therefore be potential contaminants. However, none of the samples listed possess all of the required criteria envisaged for the contaminant, therefore at present, a suitable contaminant is unidentified.

*7.2. Relationship of the SVG to the CVG*

If increases in HFSE and HREE with increasing silica in CVG rocks can be explained by highly incompatible behaviour during differentiation, then relatively low and decreasing HFSE and HREE concentrations in the SVG lavas may indicate relatively more compatible behaviour of these elements during differentiation of SVG magmas. A distinct difference in the type or abundance of phases crystallising from the magma may therefore be expected. However, there is little difference between the mineralogies of the CVG and the eastern flank SVG volcanic rocks. In contrast, the western flank SVG samples have small amounts of amphibole (hornblende) in their modal mineralogies (Table 1). Strong depletions in HREE and the steep decrease from La-Sm shown by the western flank SVG samples, relative to those with lower silica content from the eastern flank (Fig. 6), suggests that very late-stage fractionation of hornblende (± accessory phases) may account for the relatively low HREE and HFSE concentrations in these highly evolved samples (cf. deep, early-stage fractionation). The similarly shaped REE profiles and modal mineralogies of the CVG and SVG lavas with <70 wt % $SiO_2$ precludes a similar explanation for the differences observed in the geochemistry of these samples.

In addition to mineralogical differences, isotopic differences also occur between the western and eastern flank SVG lavas (Figs. 7 and 8 insets). The western vent SVG rocks are isotopically similar to the CVG group and may, therefore, be genetically related to each other, sharing a similar source and evolutionary history. The notably more primitive radiogenic isotope ratios of the eastern flank SVG lavas suggest that they may have evolved from an isotopically distinct source, or may represent the least contaminated (either by arc crust or a subduction component) Salak lava. In the latter case, they reveal the best estimate of least modified mantle wedge isotopic composition beneath Salak. The similar REE patterns of the lower $SiO_2$ SVG and lower $SiO_2$ CVG lavas (Fig. 6), suggests the magmatic source region of

the two groups probably contained a comparable mineralogy and underwent similar degrees of melting.

Trace element ratios of HFSE and HREE (e.g. Zr/Nb, Y/Nb) are often used to investigate the source characteristics of magmas (McCulloch and Gamble, 1991; Woodhead et al., 1993; Reubi and Nichols, 2004). However, the limited number of samples from the SVG, combined with the relatively differentiated nature of all Salak lavas and the uncertainty of HFSE/HREE concentrations in less differentiated samples (due to unusual increases of these elements in the CVG) hampers this approach at Salak

A schematic diagram showing the proposed evolution of magma beneath Salak is displayed in Fig. 12. Petrographic and radiogenic isotope data suggest that the high $SiO_2$ SVG rocks from the western flank vent may be related to the CVG lavas, evolving to lower HFSE and REE concentrations due to prolonged residence in the crust and the late-stage fractionation of hornblende (± accessory phases) prior to eruption (A). However, the lower $SiO_2$ (and isotopically more primitive) eastern SVG lavas are proposed to have taken a separate evolutionary pathway to the surface. Low concentrations of HFSE and HREE in these samples may be the result of fractionation of a HFSE-REE-compatible phase at depth (B), such as amphibole, which effectively inhibits the relative increase of these elements during fractional crystallisation at shallower levels. A number of factors control amphibole fractionation from magma (see Davidson et al. 2007 for a recent discussion), which include the water content of the magma and also the pressure of crystallisation. Therefore, an apparent lack of deep-seated amphibole crystallisation in the CVG may imply that the water content was not as great in the parental magma, or CVG magmas were not stored at deeper levels in the arc crust. Other arc studies that support a proposal of multiple independent conduits and reservoirs in the crust beneath active volcanoes include those of Reubi and Nicholls (2004) and Grove et al. (2005).

Within andesitic volcanic rock suites REE concentrations commonly increase with silica (Gill, 1981). Therefore, due to the relatively constant within suite REE concentrations (black crosses, Figs. 5b and h) and general lack of hornblende phenocrysts in Javan volcanic rocks, we speculate that amphibole, or other HFSE-HREE bearing phase, may fractionate at depth below most Javan volcanoes. Although amphibole-bearing xenoliths have not been found in Salak lavas, gabbroic xenoliths with variable amphibole contents are observed in lavas erupted at Sangeang Api volcano in the East Sunda arc (Turner et al., 2003) and gabbroic mafic inclusions composed of plagioclase and amphibole are present in lavas at Merapi volcano in Central Java (Camus et al., 2000).

## 8. Conclusions

Unusual HFSE and HREE variation trends (compared to most other volcanic rocks from Java) displayed by the CVG lavas of Salak are produced during differentiation in the crust. Differentiation processes have been modelled to show that: 1) CVG element variation is not consistent with simple mixing due to the low HFSE and HREE concentrations found in continental and oceanic crustal end members. 2) Evolution to high HFSE and HREE concentrations in the CVG can be explained by incompatible behaviour of these elements during fractional crystallisation. 3) Variation in some trace element ratios (K/Rb and Ba/Th) of the CVG suggest assimilation of crust also occurs during fractional crystallisation of the magma. AFC modelling and $\delta^{18}O$ data suggest that typical continental-type upper-crustal contaminants are not likely to be involved in AFC processes at Salak (cf. the Andes and Lesser Antilles, Davidson et al., 2005 and references therein). Geochemical constraints suggest that the contaminant is largely similar in geochemical and isotopic composition to the lavas themselves (e.g. volcanic and/or plutonic arc-related or ophiolitic rocks) and

characterised by $^{87}Sr/^{86}Sr \sim 0.7048$, extremely high Sr concentration and relatively low K/Rb and Ba/Th ratios.

Evolution to high HFSE and HREE concentrations in the CVG lavas suggests that magma beneath the central part of the volcano has bypassed deep-level storage in the lower crust, which is envisaged beneath the eastern flank vent. Volcanic rocks of the western flank SVG display lower HFSE and HREE contents compared to the CVG, which may be explained by relatively shallow, late-stage hornblende (± accessory phase) fractionation from a CVG-type parent.

HFSE and HREE variations in Salak lavas have drawn attention to the fact that Javan lavas do not show highly incompatible behaviour of these elements during differentiation. Y and Yb concentrations in eruptives from the volcanic front on Java display near-horizontal trends when plotted against silica. With little direct evidence of amphibole fractionation in these lavas, it is speculated that fractionation of a HFSE-HREE-compatible phase may occur at depth beneath the majority of volcanoes on Java. Tengger Caldera, in East Java also displays abnormally steep, Y, $P_2O_5$ and $TiO_2$ differentiation trends (similar to the CVG at Salak), suggesting deep-fractionation of a HFSE-HREE-compatible phase does not take place at this volcano and further corroborates the idea that the cause is related to crustal-level processes, rather than isolated source contributions at single volcanic centres in both East and West Java. This interpretation would benefit greatly from further sampling and geochemical analysis of Salak SVG deposits, to better constrain differentiation trends within this group and refine the geochemical models.

Finally, the presence of a wide HFSE and HREE variation within a single volcanic centre, such as that at Salak, emphasises the importance of detailed geochemical study of individual volcanoes. Arc lavas are generally characterised by high LREE/HFSE ratios, attributed to involvement of a subducted component. However, LREE/HFSE ratios in Salak lavas are

relatively low in the CVG, even though LREE concentrations are relatively high, due to high HSFE concentrations and positive correlations of both LREE and HFSE with $SiO_2$ in the CVG rocks.

**Acknowledgements**

We would like to thank Akhmad Zaennudin and collegues at the Volcanic Survey of Indonesia in Bandung for invaluable logistical help and guidance in the field. For technical support and analytical assistance our thanks go to: Geoff Nowell, Chris Ottley and Dave Sales at Durham University; Dave Plant at the University of Manchester; Dave Lowry at Royal Holloway University of London; Godfrey Fitton and Dodie James at the University of Edinburgh. The manuscript was greatly improved by the detailed comments of Bernard Bourdon and two anonymous reviewers. This project was funded by a NERC studentship (NER/S/A/2001/06127) and supported by the SEARG at Royal Holloway, University of London.

**References**

Alves, S., Schiano, P., Allegre, C.J., 1999. Rhenium-osmium isotopic investigation of Java subduction zone lavas. Earth Planet. Sci. Lett. 168, 65-67.

Ben-Avraham, Z., Emery, K.O., 1973. Structural framework of Sunda Shelf. Bull. Amer. Assoc. Pet. Geol. 57, 2323-2366.

Ben Othman, D.B., White, W.M., Patchett, J., 1989. The geochemistry of marine sediments, island arc magma genesis, and crust-mantle recycling. Earth Planet. Sci. Lett. 94, 1-21.

Bottazzi, P., Tiepolo, M., Vanucci, R., Zanetti, A., Brumm, R., Foley, S.F., Oberti, R., 1999. Distinct site preferences for heavy and light REE in amphibole and the prediction of Amph/LDREE. Contrib. Mineral. Petrol. 137, 36-45.

Bourdon, B., Joron, J-L, Claude-Ivanaj, C., Allègre, C.J., 1998. U-Th-Pa-Ra systematics for the Grande Comore volcanics: melting processes in an upwelling plume. Earth Planet. Sci. Lett. 164, 119-133.

Camus, G., Gourgaud, A., Mossand-Berthommier, P.C., Vincent, P.M., 2000. Merapi (Central Java, Indonesia): An outline of the structural and magmatological evolution, with a special emphasis to the major pyroclastic events. J. Volcanol. Geotherm. Res. 100, 139-163.

Carn, S.A., Pyle, D.M., 2001. Petrology and geochemistry of the Lamongan Volcanic Field, East Java, Indonesia: Primitive Sunda Arc magmas in an extensional tectonic setting? J. Petrol. 42, 1643-1683.

Charlier, B.L.A., Ginibre, C., Morgan, D., Nowell, G.M., Pearson, D.G., Davidson, J.P., Ottley, C.J., 2006. Methods for the microsampling and high-precision analysis of strontium and rubidium isotopes at single crystal scale for petrological and geochronological applications. Chem. Geol. 232, 114-133.

Chauvel, C., Blichert-Toft, J., 2001. A hafnium isotope and trace element perspective on melting of the depleted mantle. Earth Planet. Sci. Lett. 190, 137-151.

Conrad, W.K., Kay, S.M., Kay, R.W., 1983. Magma mixing in the Aleutian Arc: evidence from cognate inclusions and composite xenoliths. J. Volcanol. Geotherm. Res. 18, 279–295.

Curray, J.R., Shor Jr, G.G., Raitt, R.W., Henry, M., 1977. Seismic refraction and reflection studies of crustal structure of the eastern Sunda and western Banda arcs. J. Geophys. Res. 82, 2479-2489.

Davidson, J.P., 1987. Crustal contamination versus subduction zone enrichment: examples from the Lesser Antilles and implications for mantle source compositions of island arc volcanic rocks. Geochim. Cosmochim. Acta 51, 2185-2198.

Davidson, J.P., Dungan, M.A., Ferguson, K.M., Colucci, M.T., 1987. Crust-magma interactions and the evolution of arc magmas: The San Pedro-Pellado volcanic complex, southern Chilean Andes. Geology 15, 443-446.

Davidson, J.P., Harmon, R.S., 1989. Oxygen isotope constraints on the petrogenesis of volcanic arc magmas from Martinique, Lesser Antilles. Earth Planet. Sci. Lett. 95, 255-270.

Davidson, J.P., Hora, J.M., Garrison, J.M., Dungan, M.A., 2005. Crustal forensics in arc magmas. J. Volcanol. Geotherm. Res. 140, 157-170.

Davidson, J., Turner, S., Handley, H., Macpherson, C., Dosseto, A., 2007. Amphibole "sponge" in arc crust? Geology.35, 787-790.

Davidson, J.P., Wilson, I.R., 1989. Evolution of an alkali basalt-trachyte suite from Jebel Marra volcano, Sudan, through assimilation and fractional crystallization. Earth Planet. Sci. Lett. 95, 141-160.

de Hoog, J.C.M., Taylor, B.E., van Bergen, M.J., 2001. Sulfur isotope systematics of basaltic lavas from Indonesia: implications for the sulfur cycle in subduction zones. Earth Planet. Sci. Lett. 189, 237-252.

de Hoog, J.C.M., Koetsier, G.W., Bronto, S., Sriwana, T., Van Bergen, M.J., 2001. Sulfur and chlorine degassing from primitive arc magmas: Temporal changes during the 1982-1983 eruptions of Galunggung (West Java, Indonesia). J. Volcanol. Geotherm. Res. 108, 55-83.

DeMets, C., Gordon, R.G., Argus, D.F., Stein, S., 1990. Current plate motions. Geophysical Journal International 101, 425-478.

DePaolo, D.J., 1981. Trace element and isotopic effects of combined wallrock assimilation and fractional crystallization. Earth Planet. Sci. Lett. 53, 189-202.

Dowall, D.P, Nowell, G.M., Pearson, D.G., 2003. Chemical pre-concentration procedures for high-precision analysis of Hf-Nd-Sr isotopes in geological materials by plasma ionisation multi-collector mass spectrometry (PIMMS) techniques. Plasma Source Mass Spectrometry. Spec. Pub. Royal Society of Chemistry, 321-337.

Edwards, C.M.H., 1990. Petrogenesis of tholeiitic, calc-alkaline and alkaline volcanic rocks, Sunda arc, Indonesia. Unpublished Ph.D. Thesis, Royal Holloway, University of London, UK.

Elburg, M., Foden, J., van Bergen, M.J, Zulkarnain, I., 2005. Australia and Indonesia in collision: geochemical sources of magmatism. J. Volcanol. Geotherm. Res. 140, 25-47.

Elliot, T.R., Plank T., Zindler A., White W., Bourdon B., 1997. Element transport from slab to volcanic front at the Mariana Arc. J. Geophys. Res. B102 14991-15019

Ewart, A., 1982. The mineralogy and petrology of Tertiary-Recent orogenic volcanic rocks: with special reference to the andesitic-basaltic compositional range. In Andesites: Orogenic Andesites and Related Rocks, ed R.S. Thorpe, pp. 525-48. Wiley, Chichester.

Ewart, A.., Bryan, W. B., Chappell, B. W., Rudnick, R. L., 1994. Regional geochemistry of the Lau-Tonga arc and back-arc systems. Proc. Ocean Drilling Program, Scientific Results 135, 385-425.

Flood, T.P., Schuraytz, B.C., Vogel, T.A., 1989. Magma mixing due to disruption of a layered magma body. J. Volcanol. Geotherm. Res. 36, 241-255.

Gamble, J.A., Smith, I.E.M., McCulloch, M.T., Graham, I.J., Kokelaar, B.P., 1993. The geochemistry and petrogenesis of basalts from the Taupo volcanic zone and Kermadec island arc, S.W. Pacific. J. Volcanol. Geotherm. Res. 54, 265-290.

Gasparon, M., 1993. Origin and evolution of mafic volcanics of Sumatra (Indonesia): their mantle sources, and roles of subducted oceanic sediments and crustal contamination. Unpublished Ph.D. Thesis, Univ. Tasmania.

Gasparon, M., Hilton, D. R., Varne, R., 1994. Crustal contamination processes traced by helium isotopes: Examples from the Sunda arc, Indonesia. Earth Planet. Sci. Lett. 126, 15-22.

Gasparon, M., Varne, R., 1998. Crustal assimilation versus subducted sediment input in west Sunda arc volcanics: an evaluation. Mineralogy and Petrology 64, 89-117.

Gerbe, M.-C., Gouraud, A., Sigmarsson, O., Harmon, R.S., Joron, J-L., Provost, A., 1992. Mineralogical and geochemical evolution of the 1982-1983 Galunggung eruption (Indonesia). Bulletin of Volcanology 54, 284-298.

GERM: http://earthref.org/GERM/index.html

Gertisser, R., Keller, J., 2003a. Trace element and Sr, Nd, Pb and O isotope variations in medium-K and high-K volcanic rocks from Merapi Volcano, Central Java, Indonesia: evidence for the involvement of subducted sediments in Sunda Arc magma genesis. J. Petrol. 44, 457-489.

Gertisser, R., Keller, J., 2003b. Temporal variations in magma composition at Merapi Volcano (Central Java, Indonesia): magmatic cycles during the past 2000 years of explosive activity. J. Volcanol. Geotherm. Res. 123, 1-23.

Gill, J.B., 1981. Orogenic Andesites and Plate Tectonics. Springer, Berlin.

Grove, T.L., Baker, M.B., Price, R.C., Parman, S.W., Elkins-Tanton, L.T., Chatterjee, N., Muntener, O., 2005. Magnesian andesite and dacite lavas from Mt. Shasta, northern California: products of fractional crystallisation of H2O-rich mantle melts. Contrib. Mineral. Petrol. 148, 542-565.

Hamilton, W.B., 1979. Tectonics of the Indonesian region. U.S. Geological Survey Professional Paper reprinted with corrections, 1981 and 1985, 1078: 345.

Handley, H.K., 2006. Geochemical and Sr-Nd-Hf-O isotopic constraints on volcanic petrogenesis at the Sunda arc, Indonesia. Unpublished Ph.D. Thesis, Durham University, UK.

Handley, H.K., Macpherson, C.G., Davidson, J.P., Berlo, K., Lowry, D., 2007. Constraining fluid and sediment contributions to subduction-related magmatism in Indonesia: Ijen Volcanic Complex, Indonesia. J. Petrol. 48, 1155-1183.

Harmon, R.S., Gerbe, M.C., 1992. The 1982-83 eruption at Galunggung volcano, Java (Indonesia): oxygen isotope geochemistry of a zoned magma chamber. J. Petrol. 33, 585-609.

Hildreth, W., Moorbath, S., 1988. Crustal contributions to arc magmatism in the Andes of Central Chile. Contrib. Mineral. Petrol. 98, 455-489.

Ionov, D.A., Harmon, R.S., France-Lanord, C., Greenwood, B., Ashchepkov, I.V., 1994. Oxygen isotope composition of garnet and spinel peridotites in the continental mantle: Evidence from the Vitim xenolith suite, southern Siberia. Geochim. Cosmochim. Acta, 58, 1463-1470.

Ito, E., White, W.M., Gopel, C., 1987. The O, Sr, Nd and Pb isotope geochemistry of MORB. Chem. Geol. 62, 157-176.

Jarrard, R.D., 1986. Relations among subduction parameters. Rev. Geophys. 24, 217-284.

Kadarusman, A., Miyashita, S., Maruyama, S., Parkinson, C.D., Ishikawa, A., 2004. Petrology, geochemistry and paleogeographic reconstruction of the East Sulawesi Ophiolite, Indonesia. Tectonophysics 392, 55-83.

Kieckhefer, R.M., Shor Jr, G.G., Curray, J.R., 1980. Seismic refraction studies of the Sunda trench and forearc basin. J. Geophys. Res. 85, 863-889.

Langmuir, C.H., Voche, R.D., Hanson, G.N., Hart, S.R., 1978. A general mixing equation with applications to Icelandic basalts. Earth Planet. Sci. Lett. 37, 380-392.

Le Pichon, X., 1968. Sea-floor spreading and continental drfit. J. Geophys. Res. 73, 3661-3697.

Macpherson, C.G., Hilton, D.R., Mattey, D.P., Sinton, J.M., 2000. Evidence for an $^{18}O$-depleted mantle plume from contrasting $^{18}O/^{16}O$ ratios of back-arc lavas from the Manus Basin and Mariana Trough. Earth Planet. Sci. Lett. 176, 171-183.

Marcoux, E., Milesi, J-P., 1994. Epithermal gold deposits in West Java, Indonesia: geology, age and crustal source. Journal of Geochemical Exploration 50, 393-408.

Mattey, D., Lowry, D., Macpherson, C., 1994. Oxygen isotope composition of mantle peridotite. Earth Planet. Sci. Lett. 128, 231-241.

McCulloch, M.T., Gamble J.A., 1991. Geochemical and geodynamical constraints on subduction zone magmatism. Earth Planet. Sci. Lett. 102, 358-374.

Nowell, G.M., Kempton, P.D., Noble, S.R., Fitton, J.G., Saunders, A.D., Mahoney, J.J., Taylor, R.N., 1998. High precision Hf isotope measurements of MORB and OIB by thermal ionisation mass spectrometry: insights into the depleted mantle. Chem. Geol. 149, 211-233.

Nowell, G.M, Pearson, D.G, Ottley, C.J., Schweiters, J., 2003. Long-term performance characteristics of a plasma ionisation multi-collector mass spectrometer (PIMMS): the ThermoFinnigan Neptune. Plasma Source Mass Spectrometry. Spec. Pub. Royal Society of Chemistry, 307-320.

Ottley, C.J, Pearson, D.G., Irvine, G.J., 2003. A routine method for the dissolution of geological samples for the analysis of REE and trace elements via ICP-MS. Plasma Source Mass Spectrometry. Spec. Pub. Royal Society of Chemistry, 221-230.

Patchett, P.J., 1983. Hafnium isotope results from mid-ocean ridges and Kerguelen. Lithos 16, 47-51.

Patchett, P.J., Tatsumoto, M., 1980. Hafnium isotope variations in oceanic basalts. Geophys. Res. Lett. 7, 1077-1080.

Pearce, J.A., 1982. Trace element characteristics of lavas from destructive plate boundaries. Andesites: Orogenic Andesites and Related Rocks. John Wiley & Sons, Chichester, UK, 525-548.

Pearce, J.A., Kempton, P.D., Nowell, G.M., Noble, S.R., 1999. Hf-Nd Element and Isotope Perspective on the Nature and Provenance of Mantle and Sunduction Components in Western Pacific Arc-Basin Systems. J. Petrol. 40, 1579-1611.

Price, R.C., Kennedy, A.K., Riggs-Sneeringer, M., Frey, F.A., 1986. Geochemistry of basalts from the Indian Ocean triple junction: implications for the generation and evolution of Indian Ocean ridge basalts. Earth Planet. Sci. Lett. 78, 379-396.

Rapp, R.P., Watson, E.B., 1995. Dehydration melting of a metabasalt at 8-32 kbar: Implications for continental growth and crustal recycling. J. Petrol. 36, 891-931.

Rehkämper, M., Hofmann, A.W., 1997. Recycled ocean crust and sediment in Indian Ocean MORB. Earth Planet. Sci. Lett. 147, 93-106.

Reubi, O., Nicholls, I.A., 2004. Magmatic evolution at Batur volcanic field, Bali, Indonesia: petrological evidence for polybaric fractional crystallisation and implications for caldera-forming eruptions. J. Volcanol. Geotherm. Res. 138, 345-369.

Reubi, O., Nicholls, I.A., Kamenetsky, V.S., 2002. Early mixing and mingling in the evolution of basaltic magmas: evidence from phenocryst assemblages, Slamet Volcano, Java, Indonesia. J. Volcanol. Geotherm. Res. 119, 255-274.

Royse, K., Kempton, P.D., Darbyshire, D.P.F., 1998. NERC Isotope Geosciences Laboratory Report Series, 121.

Salters, V.J.M., 1996. The generation of mid-ocean ridge basalts from the Hf and Nd isotope perspective. Earth Planet. Sci. Lett. 141, 109-123.

Salters, V.J.M., Hart, S.R., 1991. The mantle sources of ocean islands and arc basalts: the Hf isotope connection. Earth Planet. Sci. Lett. 104, 364-380.

Salters, V.J.M., White, W.M., 1998. Hf isotope constraints on mantle evolution. Chem. Geol. 145, 447-460.

Sitorus, K., 1990. Volcanic stratigraphy and geochemistry of the Idjen Caldera Complex, East Java, Indonesia, MSc thesis, University of Wellington, New Zealand.

Staudigel, H., Plank, T., White, B., Schimincke, H-U., 1996. Geochemical fluxes during seafloor alteration of the basaltic upper oceanic crust: DSDP Sites 417 and 418, Subduction: Top to Bottom. Geophysical Monograph 96, pp. 19-36.

Stille, P., Unruh, D.M., Tatsumoto, M., 1986. Pb, Sr, Nd, and Hf isotopic constraints on the origin of Hawaiian basalts and evidence for a unique mantle source. Geochim. Cosmochim. Acta 50, 2303-2319.

Stimac, J., 2003. Surface geology of the Awibengkok geothermal development area, Java, Indonesia. Unocal report, Philippines.

Stormer, J. C., Jr., Nicholls, J., 1978. XLFRAC; a program for the interactive testing of magmatic differentiation models. Computers & Geosciences 4, 143-159.

Sun, S., McDonough, W.F., 1989. Chemical and isotopic systematics of oceanic basalts: implications for mantle composition and processes. In: A.D. Saunders, Norry, M.J. (Editor), Magmatism in the Ocean Basins. Geological Society Special Publication, 313-345.

Taylor, S.R., 1977. Island arc models and the composition of the continental crust, in Talwani, M., Pitman, W., eds., Island arcs, deep sea trenches and back arc basins: American Geophysical Union, Maurice Ewing Series 1, 325-335.

Tepley, F.J., III, Davidson, J.P., Tilling, R.I., Arth, J.G., 2000. Magma mixing, recharge and eruption histories recorded in plagioclase phenocrysts from El Chichon, Mexico. J. Petrol. 41, 1397-1411.

Thirlwall, M.F., 1991. Long-term reproducibility of multicollector Sr and Nd isotope ratio analysis. Chem. Geol.; Isotope Geoscience Section 94, 85-104.

Thirlwall, M.F., Graham A.M., Arculus R.J., Harmon R.S., Macpherson C.G., 1996. Resolution of the effect of crustal assimilation, sediment subduction and fluid transport in island arc magmas: Pb-Sr-Nd-O isotope geochemistry of Grenada, Lesser Antilles. Geochim. Cosmochim. Acta 60, 4785-4810.

Tregoning, P., Brunner, F.K., Bock, Y., Puntodewo, S.S.O., McCaffrey, R., Genrich, J.F., Calais, E., Rais, J., Subarya, C., 1994. First geodetic measurement of convergence across the Java Trench. Geophys. Res. Lett. 21, 2135-2138.

Turner, S., Foden. J, George, R., Evans, P., Varne, R., Elburg, M., Jenner, G., 2003. Rates and processes of potassic magma evolution beneath Sangeang Api volcano, East Sunda Arc, Indonesia. J. Petrol. 44, 491-515.

Turner, S., Hawkesworth, C., Rogers, N., Bartlett, J., Worthington, T., Hergt, J., Pearce, J., Smith, I., 1997. $^{238}U$-$^{230}Th$ disequilibria, magma petrogenesis and flux rates beneath the depleted Tonga-Kermadec island arc. Geochim. Cosmochim. Acta 61, 4855-4884.

van Gerven, M., Pichler, H., 1995. Some aspects of the volcanology and geochemistry of the Tengger Caldera, Java, Indonesia: eruption of a K-rich tholeiitic series. Journal of Southeast Asian Earth Sciences 11, 125-133.

Vervoort, J.D., Patchett, P.J., Blichert-Toft, J., Albarede, F., 1999. Relationships between Lu-Hf and Sm-Nd isotopic systems in the global sedimentary system. Earth Planet. Sci. Lett. 168, 79-99.

Vogel, T.A., 1982. Magma mixing in the acidic-basic complex of Ardnamurchan; implications on the evolution of shallow magma chambers. Contrib. Mineral. Petrol. 79, 411-423.

Vukadinovic, D., Sutawidjaja, I., 1995. Geology, mineralogy and magma evolution of Gunung Slamet Volcano, Java, Indonesia. Journal of Southeast Asian Earth Sciences, 11, 135-164.

White, W.M., Patchett, J., 1984. Hf-Nd-Sr isotopes and incompatible element abundances in island arcs: implications for magma origins and crustal-mantle evolution. Earth Planet. Sci. Lett. 67, 167-185.

White, W.M., Patchett, J., Ben Othman, D., 1986. Hf isotope ratios of marine sediments and Mn nodules; evidence for a mantle source of Hf in seawater. Earth Planet. Sci. Lett. 79, 46-54.

Whitford, D.J., White, W.M., Jezek, P.A., 1981. Neodymium isotopic composition of Quaternary island arc lavas from Indonesia. Geochim. Cosmochim. Acta 45, 989-995.

Woodhead, J.D., 1989. Geochemistry of the Mariana Arc (Western Pacific): Source composition and processes, Chem. Geol. 76, 1-24.

Woodhead, J.D., Eggins, S.M., Gamble, J., 1993. High field strength and transition element systematics in island arc and back-arc basin basalts: evidence for multi-phase melt extraction and depleted mantle wedge. Earth Planet. Sci. Lett. 114, 491-504.

Woodhead, J.D., Hergt, J.M., Davidson, J.P., Eggins, S.M., 2001. Hafnium isotope evidence for ‘conservative’ element mobitiy during subduction processes. Earth Planet. Sci. Lett. 192, 331-346.

Zaennudin, A., Sutawidjaja, I.S., Aswin, D., 1993. Geological map of Salak Volcano, West Java. Volcanic Survey of Indonesia, Indonesia.

Zellmer G.F., Hawkesworth, C.J., Sparks, R.S.J., Thomas, L.E., Harford, C.L., Brewer, T.S., Loughlin, S.C., 2003. Geochemical evolution of the Soufriere Hills Volcano, Montserrat, Lesser Antilles Volcanic Arc. J. Petrol. 44, 1349-1374.

**Figure Captions**

Fig. 1. Topographic sketch map of the Salak-Perbakti-Gagak Complex, showing the distribution of samples used in this study and corresponding data symbols used on subsequent figures. CVG = Central Vent Group; SVG = Side Vent Group; SL3 = Salak lava 3 (Zaennudin et al., 1993). Selected rivers are shown in black dash; solid lines with ticks represent escarpments. Inset diagram shows the location of Salak (large black triangle) in West Java, in relation to major centres of population (grey fill) and Quaternary volcanoes (small black triangles).

Fig. 2. Analyses of pyroxene phenocrysts in Salak lavas. Dashed lines represent 10% increments.

Fig. 3. Compositional variation of plagioclase phenocrysts in Salak volcanic rocks. Grey lines represent 10% increments.

Fig. 4. Major element variation diagrams for Salak volcanic rocks. Tengger Caldera (open circles) distinguished from the other Java volcanic data (small crosses) to highlight the unusual geochemical properties of the rocks (data from van Gerven & Pichler, 1995). Java data: B, Bayah Dome (Marcoux and Milesi, 1994; Alves et al., 1999); C, Cereme (Edwards, 1990); G, Gede Volcanic Complex (Handley, 2006); Ga, Galunggung (Gerbe et al., 1992; de Hoog et al., 2001); Gu, Guntur (Edwards, 1990; de Hoog et al., 2001); I, Ijen Volcanic

Complex (Handley et al., 2007); M, Merapi (Gertisser and Keller, 2003a); S, Slamet (Vukadinovic and Sutawidjaja, 1995; Reubi and Nicholls, 2002). Model fractionation curves are shown for removal of the mineral assemblage suggested by least squares modelling from S106B (model 1) in Table 9: 0.7 Plag, 0.1 Cpx, 0.13 Opx, 0.07 Fe-Ti oxide. Mineral data used in modelling is given in Tables 3-5. Fractionation curves are labelled with the percentage of melt remaining.

Fig. 5. Selected trace element variations with $SiO_2$ for Salak volcanic rocks. Java data sources as in Fig. 4. SVG samples erupted from eastern flank (E. Flank) and western flank (W. Flank) vents are indicated in b). Model fractionation curves (FC) are shown for 100% amphibole fractionation (crosses) from Javan basalt (Ijen Volcanic Complex KI69, Handley et al., 2007) using mineral partition coefficients from Bottazzi et al. (1999) and mineral composition from Rapp and Watson at 8kbar, 1000ºC (1995), and for fractionation of the mineral assemblage suggested by least squares modelling (horizontal ticks) see Fig. 4 for details. Curves are labelled with the percentage of melt remaining.

Fig. 6. Chondrite normalised rare earth element diagram of Salak rocks. Normalising factors and Normal (N)-MORB values from Sun and McDonough (1989). Indian (I)-MORB (Chauvel and Blichert-Toft, 2001).

Fig. 7. Variation of $^{143}Nd/^{144}Nd$ with $^{87}Sr/^{86}Sr$ for Salak volcanic rocks. Data sources: I-MORB: Rehkämper and Hofmann, 1997; Ito et al., 1987; Price et al., 1986; Chauvel and Blichert-Toft, 2001; N-MORB: Ito et al., 1987; Chauvel and Blichert-Toft, 2001; Java: White and Patchett, 1984; Whitford et al, 1981; Edwards, 1990; Gertisser and Keller, 2003a; Gerbe et al, 1992; Handley et al., 2007; Handley, 2006; Indian ocean sediments: Ben Othman et al.,

1989; Gasparon and Varne, 1998. Inset: Nd and Sr isotope ratio diagram separated by group. 2σ external errors shown for each analysis. E. Flank = eastern flank vent samples S102 and S103.

Fig. 8. $^{176}Hf/^{177}Hf$ - $^{143}Nd/^{144}Nd$ variation in Salak volcanic rocks. Data sources: I-MORB: Salters, 1996; Nowell et al., 1998; Chauvel and Blichert-Toft, 2001; N-MORB: I-MORB refs. and Salters and Hart, 1991; OIB: Salters and Hart, 1991; Salters and White, 1998; Nowell et al., 1998; Patchett and Tatsumoto, 1980; Patchett, 1983; Stille et al., 1986; Java: White and Patchett, 1983; Woodhead et al., 2001; Handley et al., 2007; Handley, 2006; Banda: White and Patchett, 1984; Indian ocean sediments: Ben Othman et al., 1989; White et al., 1986; Vervoort et al., 1999. Dividing line for Indian and Pacific MORB provenance from Pearce et al., 1999. Inset: Hf-Nd isotope diagram of Salak volcanic rocks separated by group. 2σ external errors shown for each analysis on the inset diagram. E. Flank = eastern flank vent samples S102 and S103.

Fig. 9. a) K/Rb-Rb and b) Ba/Th-Y, showing fractional crystallisation (FC), combined assimilation and fractional crystallisation (AFC A, B and C), and bulk mixing (MM A, B, C and D) curves for models involving Salak basaltic andesite S106B and A: rhyolite (this study), B & D: Seputih granite plutonics 75415 and 75413 respectively (southern Sumatra, Gasparon, 1993) and C: Javan arc tholeiite from Guntur, GU1/T (Edwards, 1990). See Table 8 for end member compositions. Tick marks on FC and AFC curves indicate the percentage of liquid remaining. Tick marks on mixing curves represent the percentage of A, B, C or D mixed with the magma. FC and AFC calculations use the mineral proportions suggested by least squares major element modelling of CVG rocks S106B to S110B (Table 9, model 1): Plag = 0.7; Cpx = 0.1; Opx = 0.13; Oxide = 0.07. AFC curves calculated using DePaolo

(1981). The rate ratio (r) of mass assimilated to mass crystallised in AFC model: A = 0.5, B = 0.05, C = 0.8.

Fig. 10. Variation of $^{87}Sr/^{86}Sr$ isotope ratio versus $SiO_2$ for Salak volcanic rocks. Arrows labelled SH, AFC and FC indicate the hypothesised data trends related to: heterogeneity in the mantle source (SH), combined assimilation and fractional crystallisation (AFC) and fractional crystallisation (FC). Inset shows Th/Ba versus $SiO_2$ for Salak rocks, highlighting the similar differentiation patterns between Th/Ba and $^{87}Sr/^{86}Sr$ and suggesting the former, for which there is more data, might serve as a proxy for isotopic composition.

Fig. 11. Ba/Th against $^{87}Sr/^{86}Sr$ for Salak volcanic rocks. FC and AFC curves are shown for the same models (AFC A, B and C) in Fig. 9 (see caption for details). $^{87}Sr/^{86}Sr$ ratios used in model AFC C is that of GU2/C (Edwards, 1990). Arrow labelled FC indicates differentiation trend expected from fractional crystallisation alone. Tick marks on FC and AFC curves indicate the percentage of liquid remaining.

Fig. 12. Schematic representation of magmatic evolution, showing the multiple magma storage areas and pathways envisaged in petrogenesis at Salak. (A) and (B) relate to discussion in the text: (A) indicates continued magmatic evolution from a CVG-type parent at shallow depth, involving late-stage fractionation of hornblende in petrogenesis of the western flank SVG rocks, (B) indicates hypothesised fractionation of a HFSE-HREE compatible phase at depth in the evolution of SVG magma below the eastern flank vent.

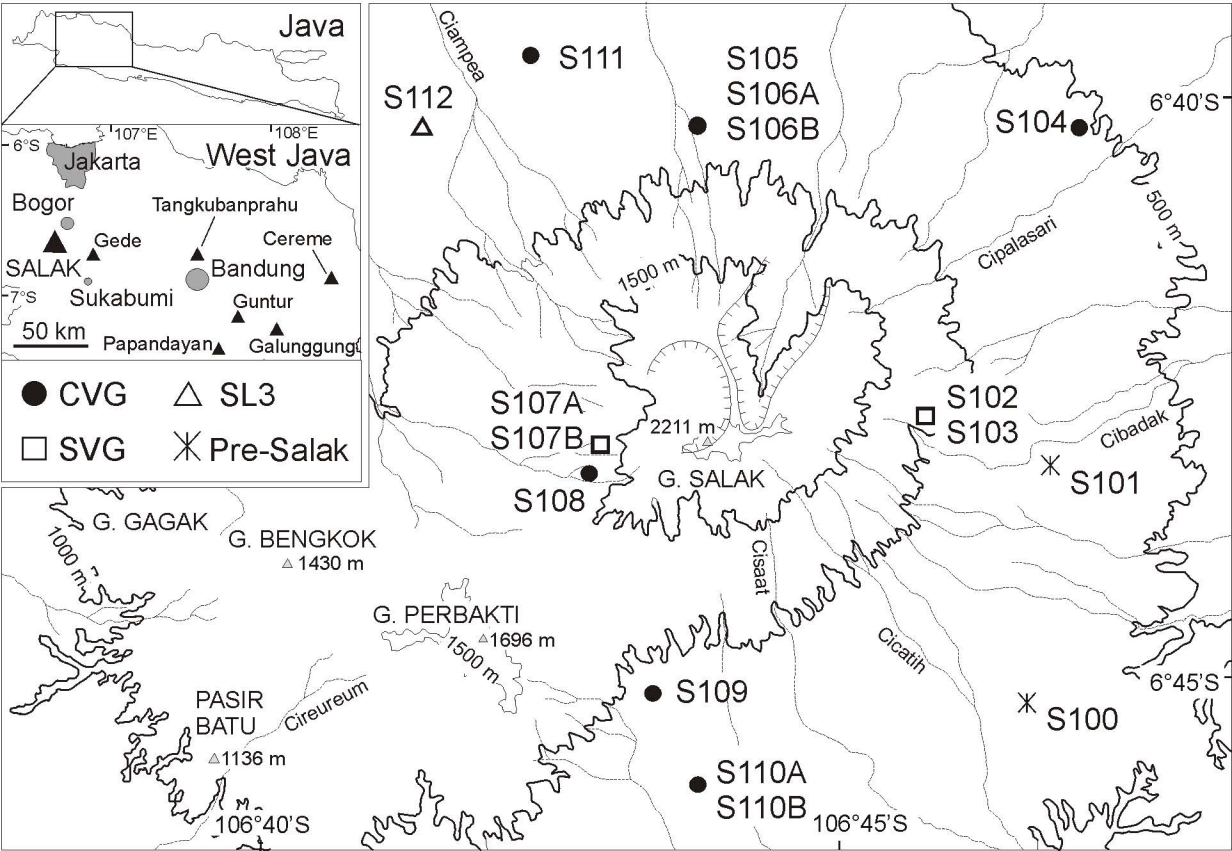
Java
107°E
108°E
6°S
Jakarta
West Java
Bogor
Tangkubanprahu
Gede
Cereme
SALAK
Bandung
7°S
Sukabumi
Guntur
50 km
Papandayan
Galunggung
CVG
SL3
SVG
Pre-Salak
Ciampea
S111
S112
S105
S106A
S106B
S104
6°40'S
500 m
Cipalasari
1500 m
S107A
S107B
2211 m
S102
S103
Cibadak
S101
S108
G. SALAK
G. GAGAK
G. BENGKOK
1430 m
1000 m
Cisaat
G. PERBAKTI
1696 m
1500 m
Cicatih
6°45'S
PASIR
BATU
1136 m
Cireureum
S109
S100
S110A
S110B
106°40'S
106°45'S

Wo

CVG

Basaltic Andesite S106B

Andesite S110B

a)

En

Fs

Wo

SVG

Andesite S102

Xenolith in Andesite

b)

En

Fs

Wo

SL3

Andesite S112

c)

En

Fs

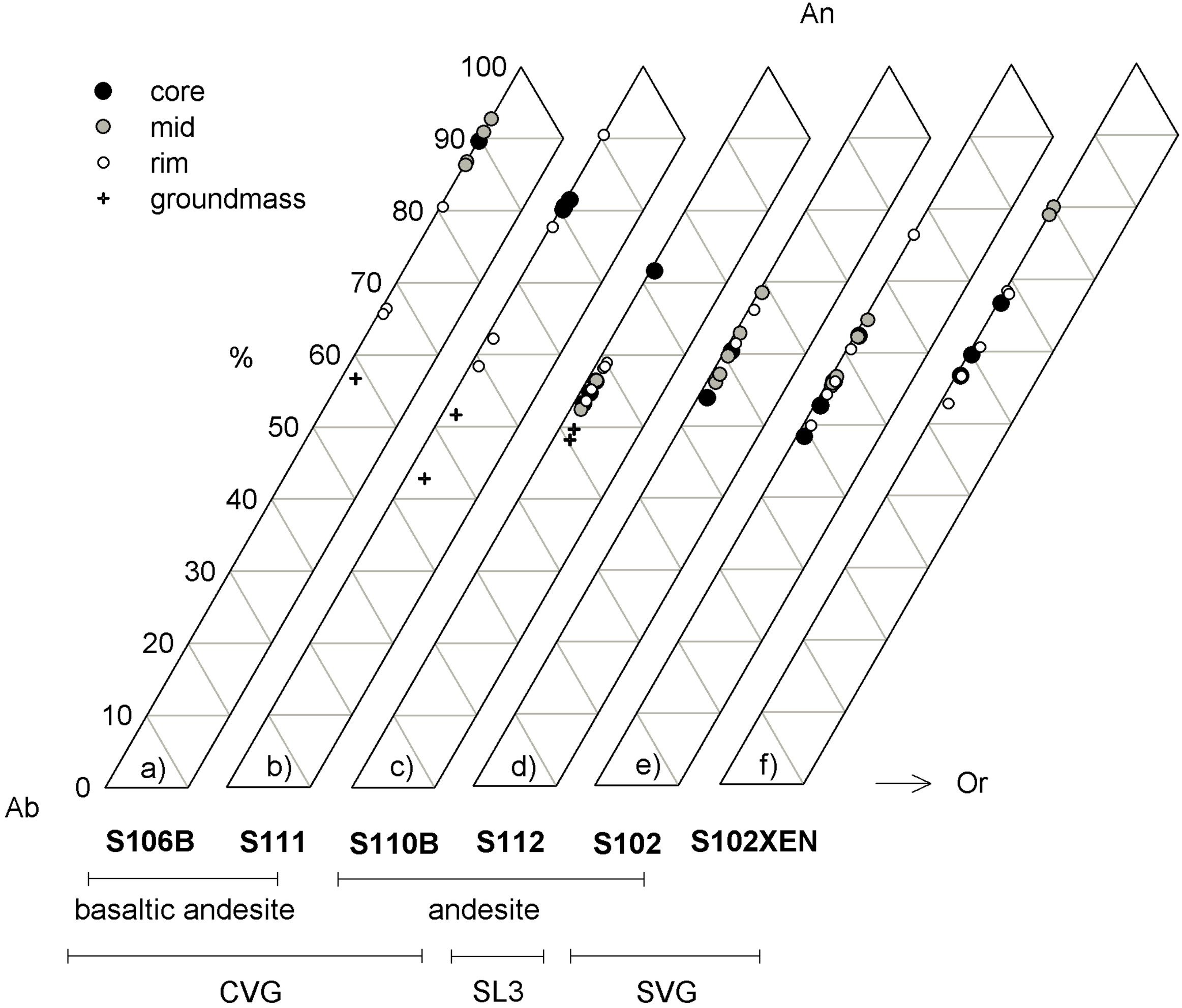
An
core
mid
rim
groundmass
100
90
80
70
60
50
40
30
20
10
0
%
a)
b)
c)
d)
e)
f)
Ab
Or
S106B
S111
S110B
S112
S102
S102XEN
basaltic andesite
andesite
CVG
SL3
SVG

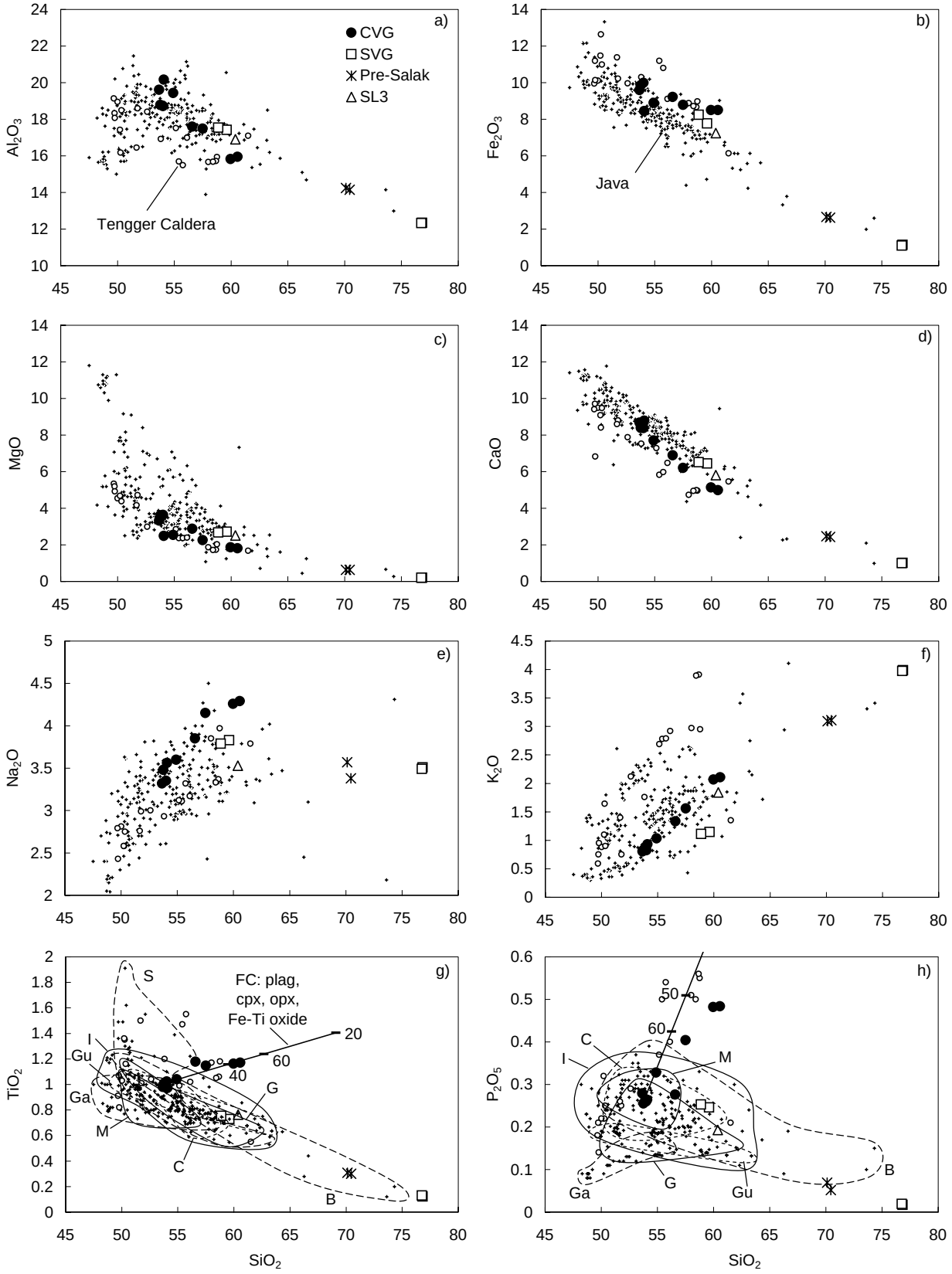
a)
CVG
SVG
Pre-Salak
SL3
Tengger Caldera
Al2O3
b)
Java
Fe2O3
c)
MgO
d)
CaO
e)
Na2O
f)
K2O
g)
S
FC: plag,
cpx, opx,
Fe-Ti oxide
20
40
60
I
Gu
Ga
M
G
C
B
TiO2
SiO2
h)
50
60
C
I
M
Ga
G
Gu
B
P2O5
SiO2

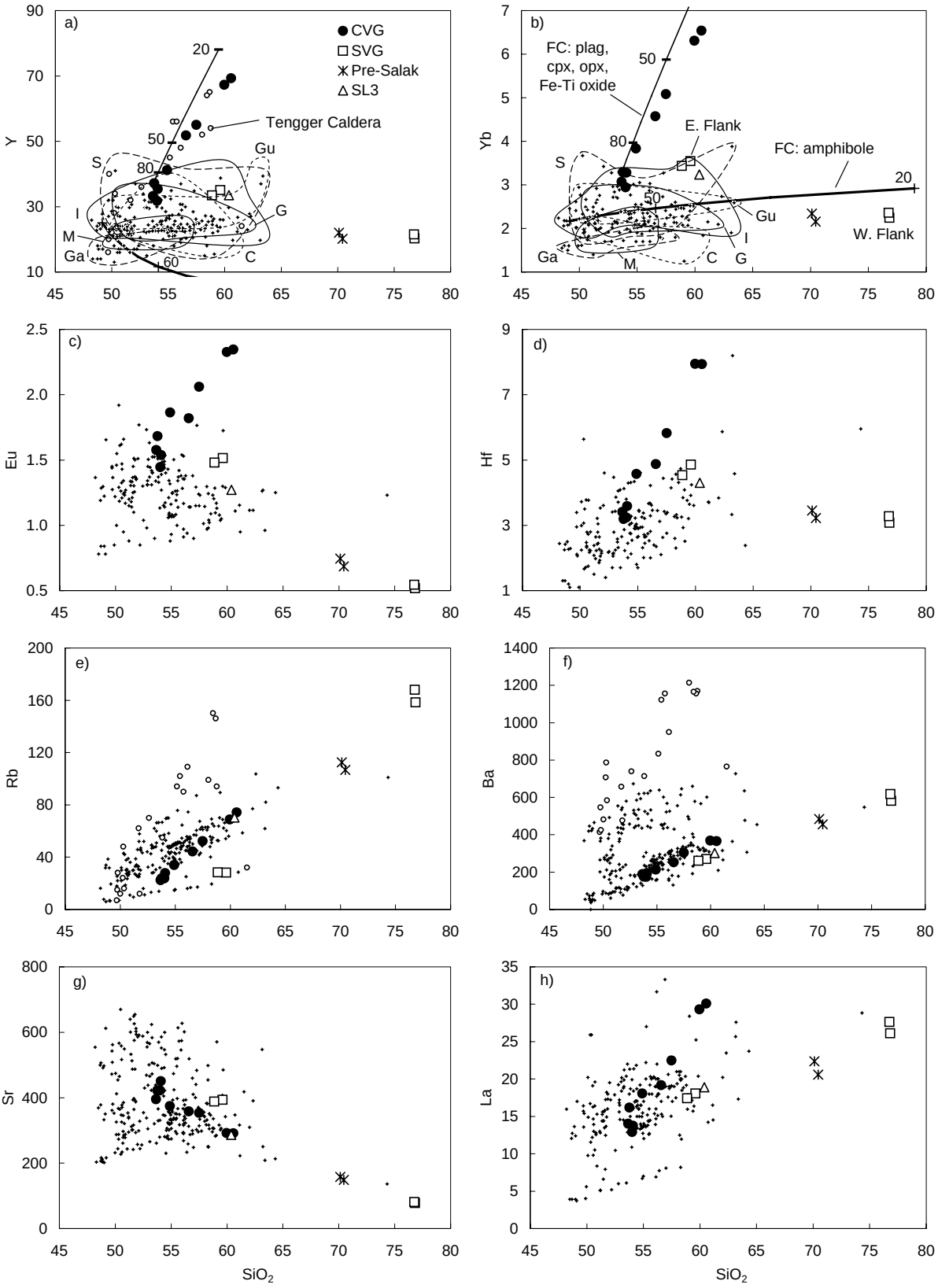
a)
CVG
SVG
Pre-Salak
SL3
Tengger Caldera
20
50
80
60
S
I
M
Ga
Gu
G
C
Y
b)
FC: plag,
cpx, opx,
Fe-Ti oxide
E. Flank
FC: amphibole
W. Flank
Yb
c)
Eu
d)
Hf
e)
Rb
f)
Ba
g)
Sr
h)
La
SiO2
SiO2

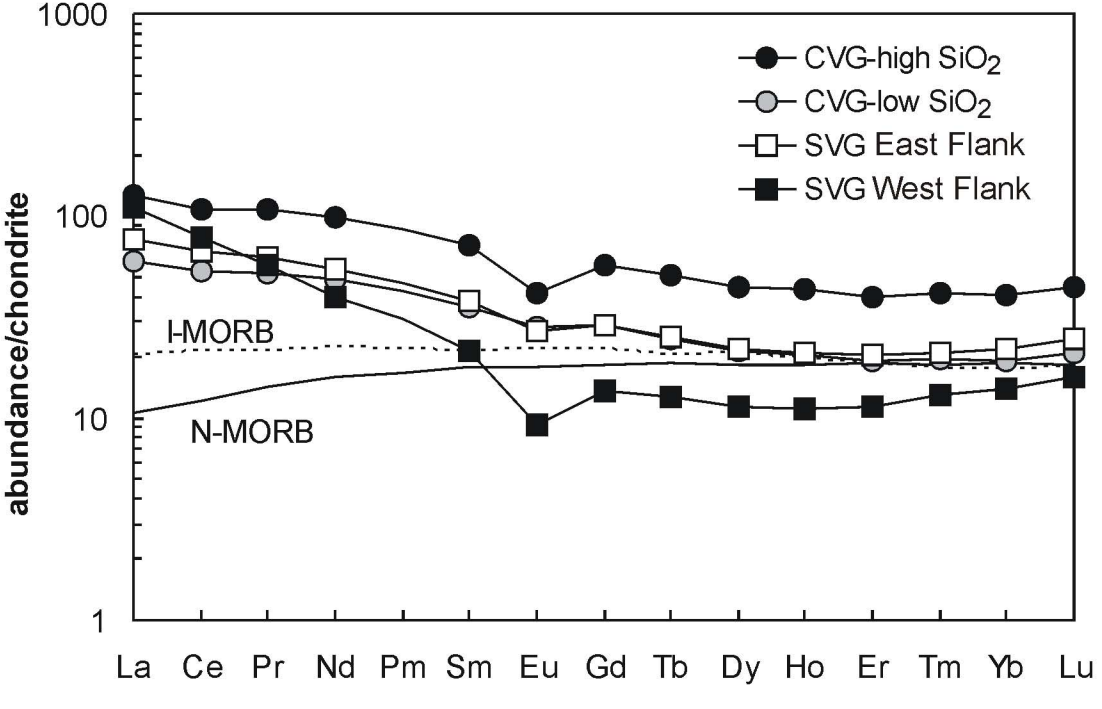
1000
100
10
1
abundance/chondrite
CVG-high SiO2
CVG-low SiO2
SVG East Flank
SVG West Flank
I-MORB
N-MORB
La
Ce
Pr
Nd
Pm
Sm
Eu
Gd
Tb
Dy
Ho
Er
Tm
Yb
Lu

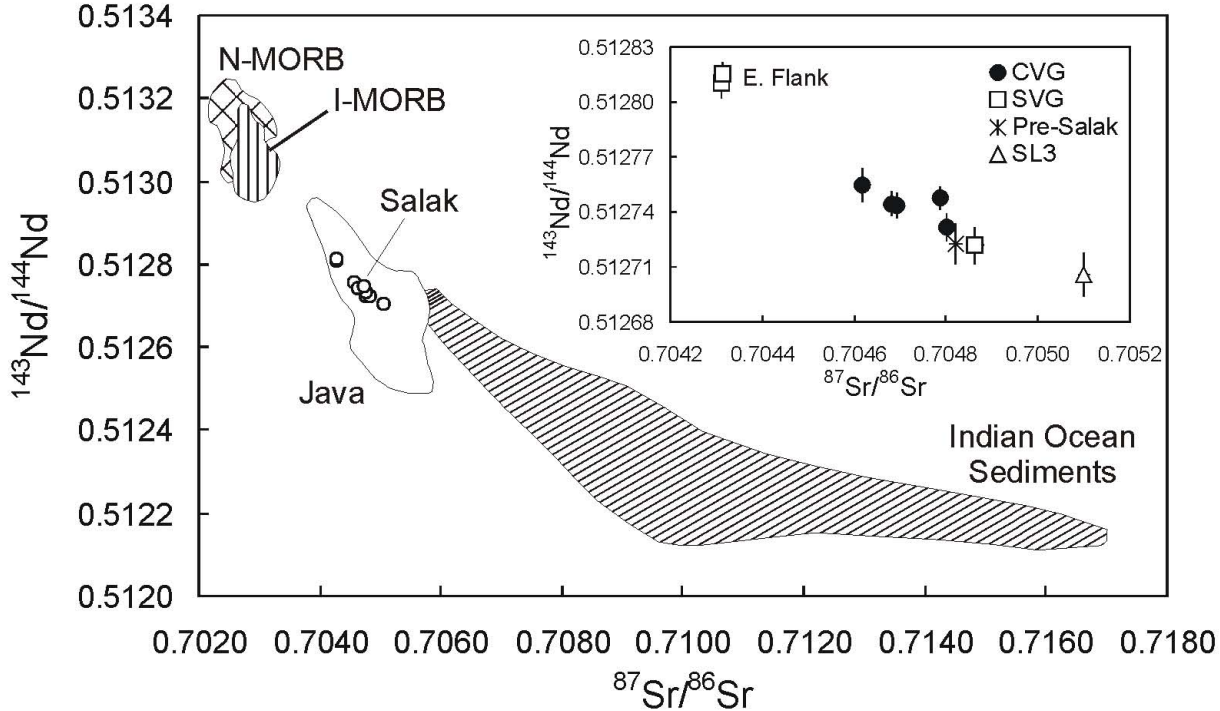
N-MORB
I-MORB
Salak
Java
Indian Ocean
Sediments
E. Flank
CVG
SVG
Pre-Salak
SL3
$^{143}Nd/^{144}Nd$
$^{87}Sr/^{86}Sr$
0.5134
0.5132
0.5130
0.5128
0.5126
0.5124
0.5122
0.5120
0.7020
0.7040
0.7060
0.7080
0.7100
0.7120
0.7140
0.7160
0.7180
0.51283
0.51280
0.51277
0.51274
0.51271
0.51268
0.7042
0.7044
0.7046
0.7048
0.7050
0.7052

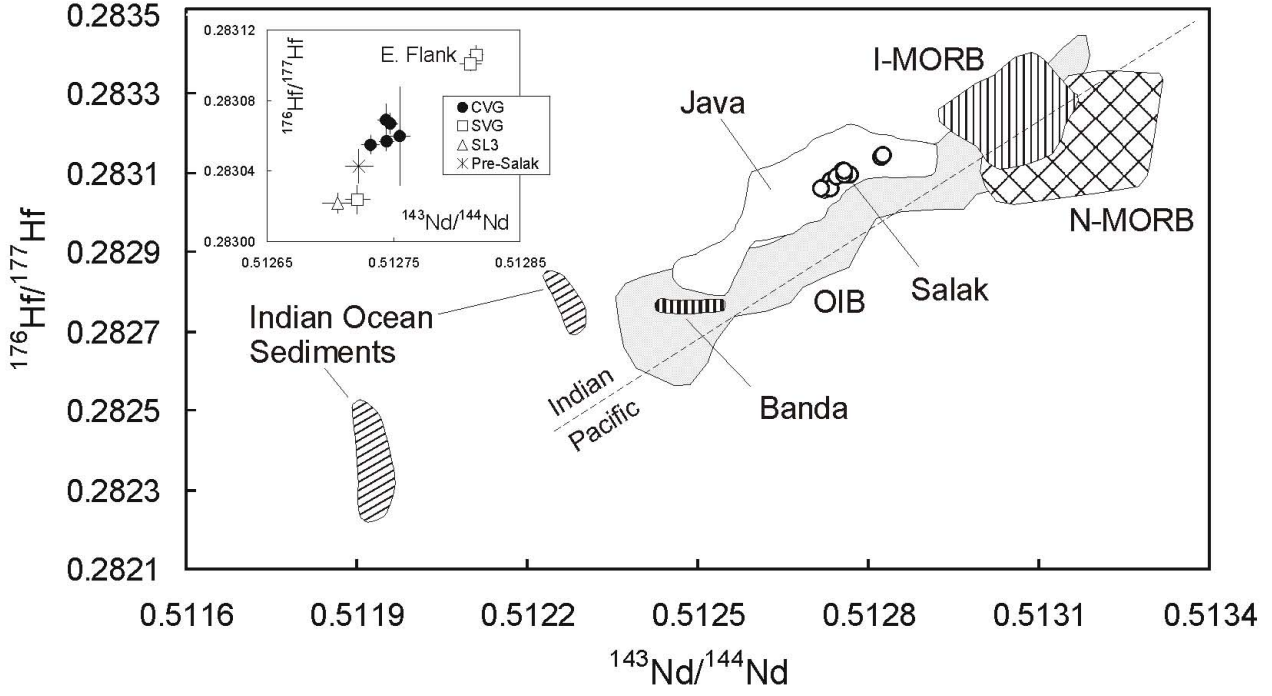
0.2835
0.2833
0.2831
0.2829
0.2827
0.2825
0.2823
0.2821
$^{176}Hf/^{177}Hf$
0.5116
0.5119
0.5122
0.5125
0.5128
0.5131
0.5134
$^{143}Nd/^{144}Nd$
I-MORB
Java
N-MORB
Salak
OIB
Banda
Indian Ocean
Sediments
Indian
Pacific
E. Flank
CVG
SVG
SL3
Pre-Salak
0.28312
0.28308
0.28304
0.28300
0.51265
0.51275
0.51285

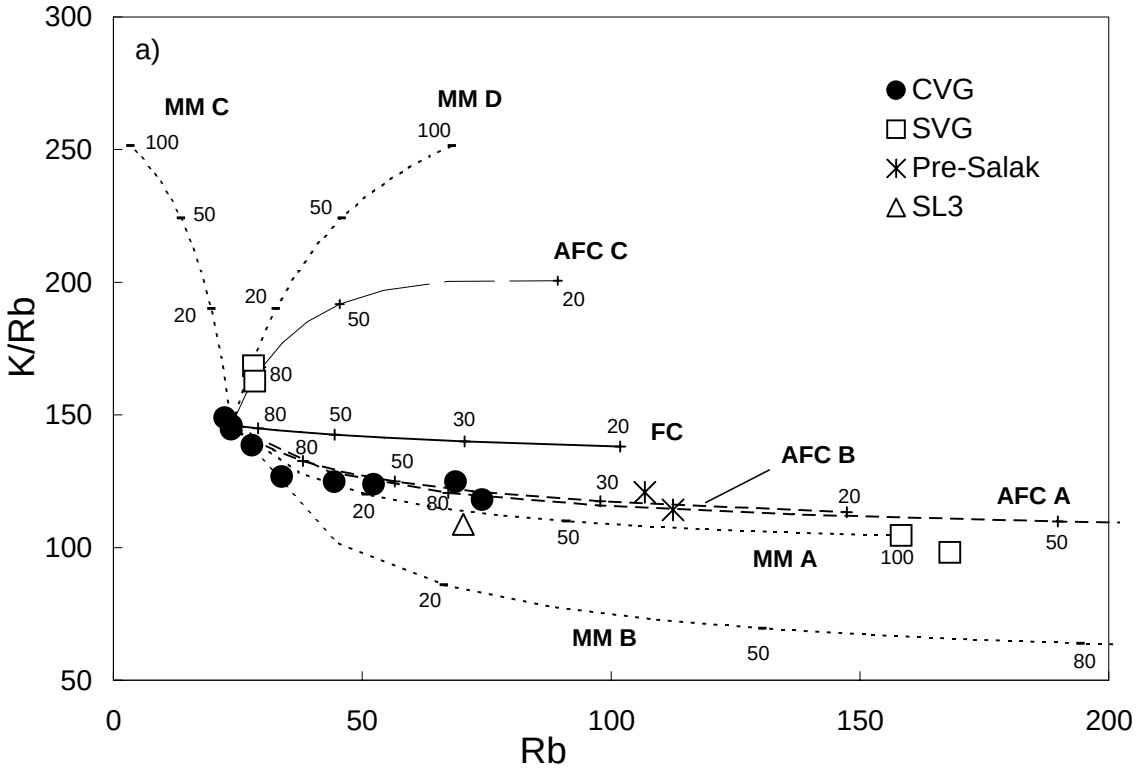
a)
CVG
SVG
Pre-Salak
SL3
MM C
MM D
AFC C
FC
AFC B
AFC A
MM A
MM B
K/Rb
Rb
300
250
200
150
100
50
0
50
100
150
200

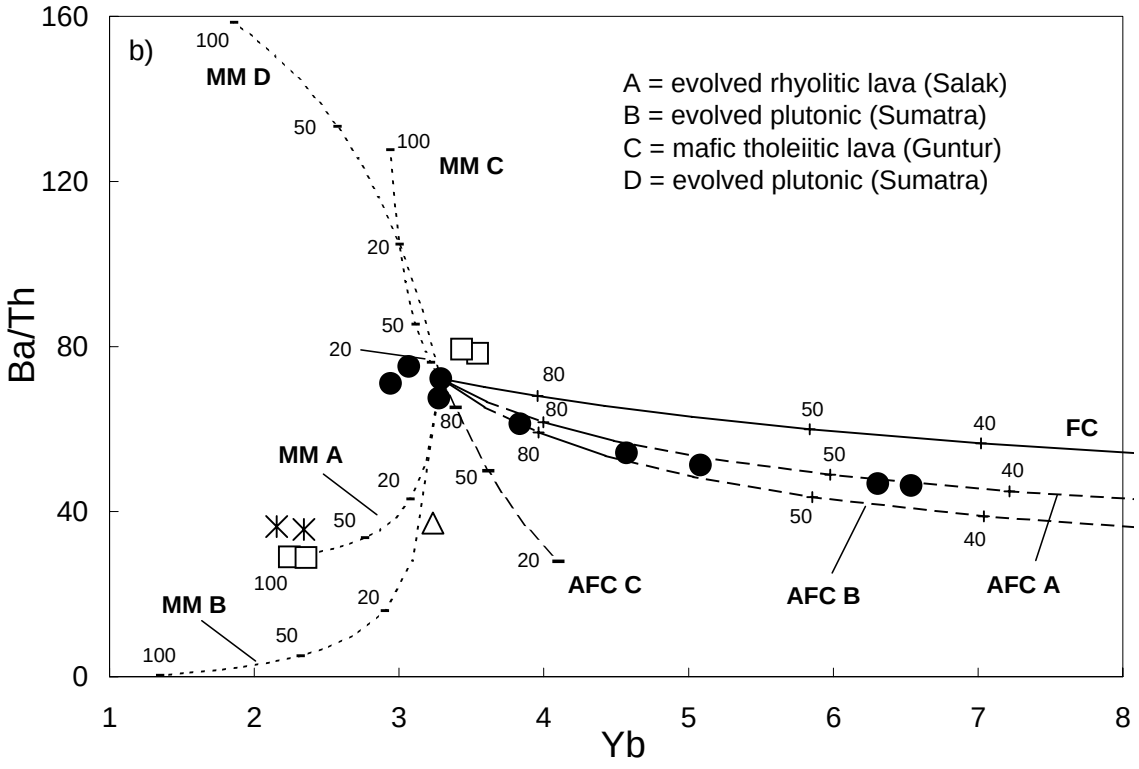
b)
A = evolved rhyolitic lava (Salak)
B = evolved plutonic (Sumatra)
C = mafic tholeiitic lava (Guntur)
D = evolved plutonic (Sumatra)
MM D
MM C
MM A
MM B
AFC C
AFC B
AFC A
FC
Ba/Th
Yb
160
120
80
40
0
1
2
3
4
5
6
7
8

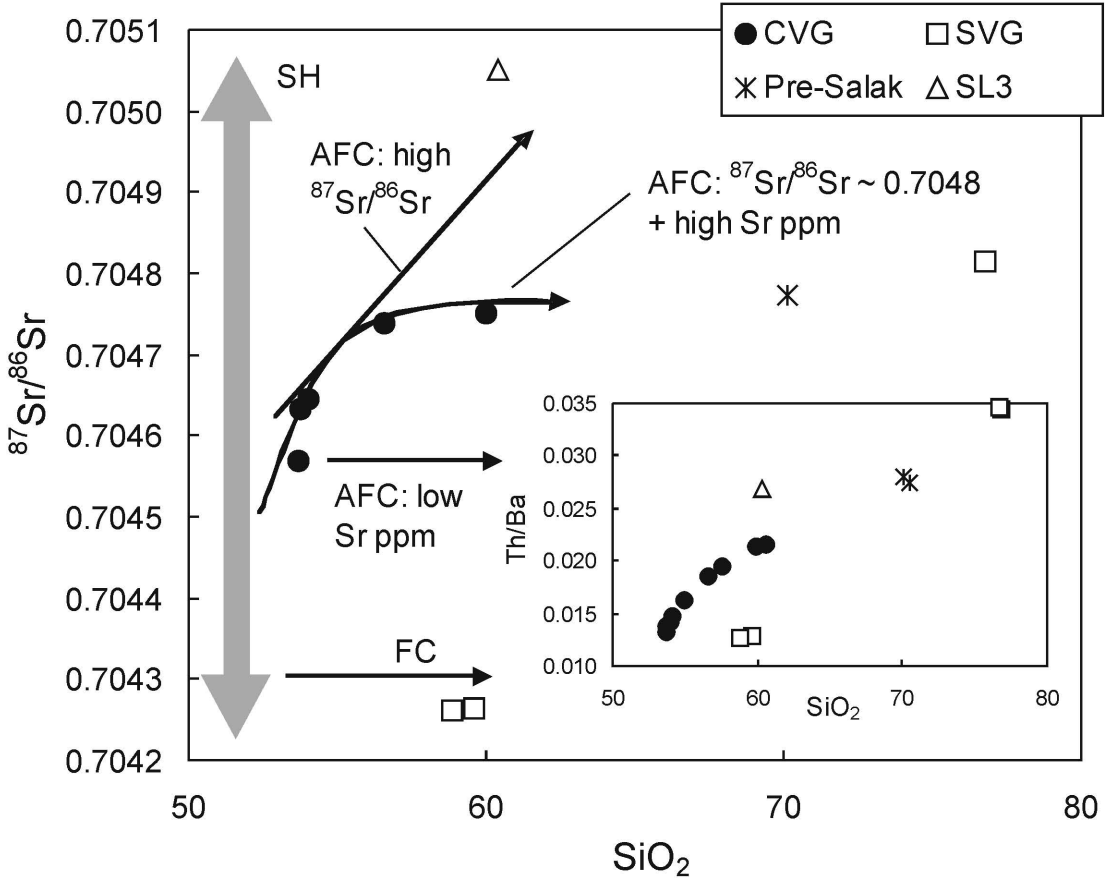
CVG
SVG
Pre-Salak
SL3
SH
AFC: high
87Sr/86Sr
AFC: 87Sr/86Sr ~ 0.7048
+ high Sr ppm
AFC: low
Sr ppm
FC
87Sr/86Sr
SiO2
Th/Ba
0.7051
0.7050
0.7049
0.7048
0.7047
0.7046
0.7045
0.7044
0.7043
0.7042
50
60
70
80
0.035
0.030
0.025
0.020
0.015
0.010

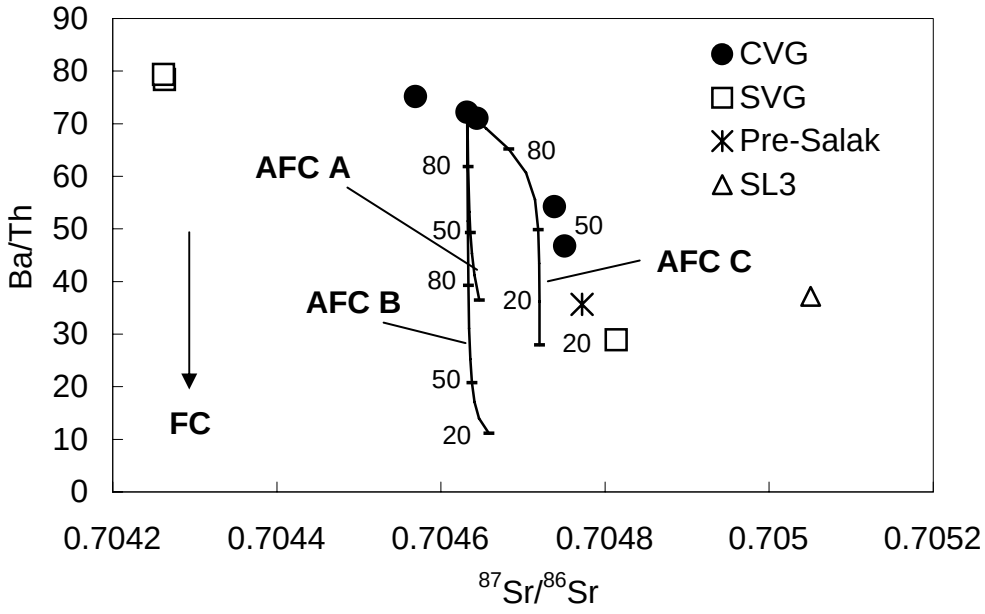
90
80
70
60
50
40
30
20
10
0
Ba/Th
0.7042
0.7044
0.7046
0.7048
0.705
0.7052
87Sr/86Sr
CVG
SVG
Pre-Salak
SL3
AFC A
AFC B
AFC C
FC
80
50
20
80
50
20
80
50
20

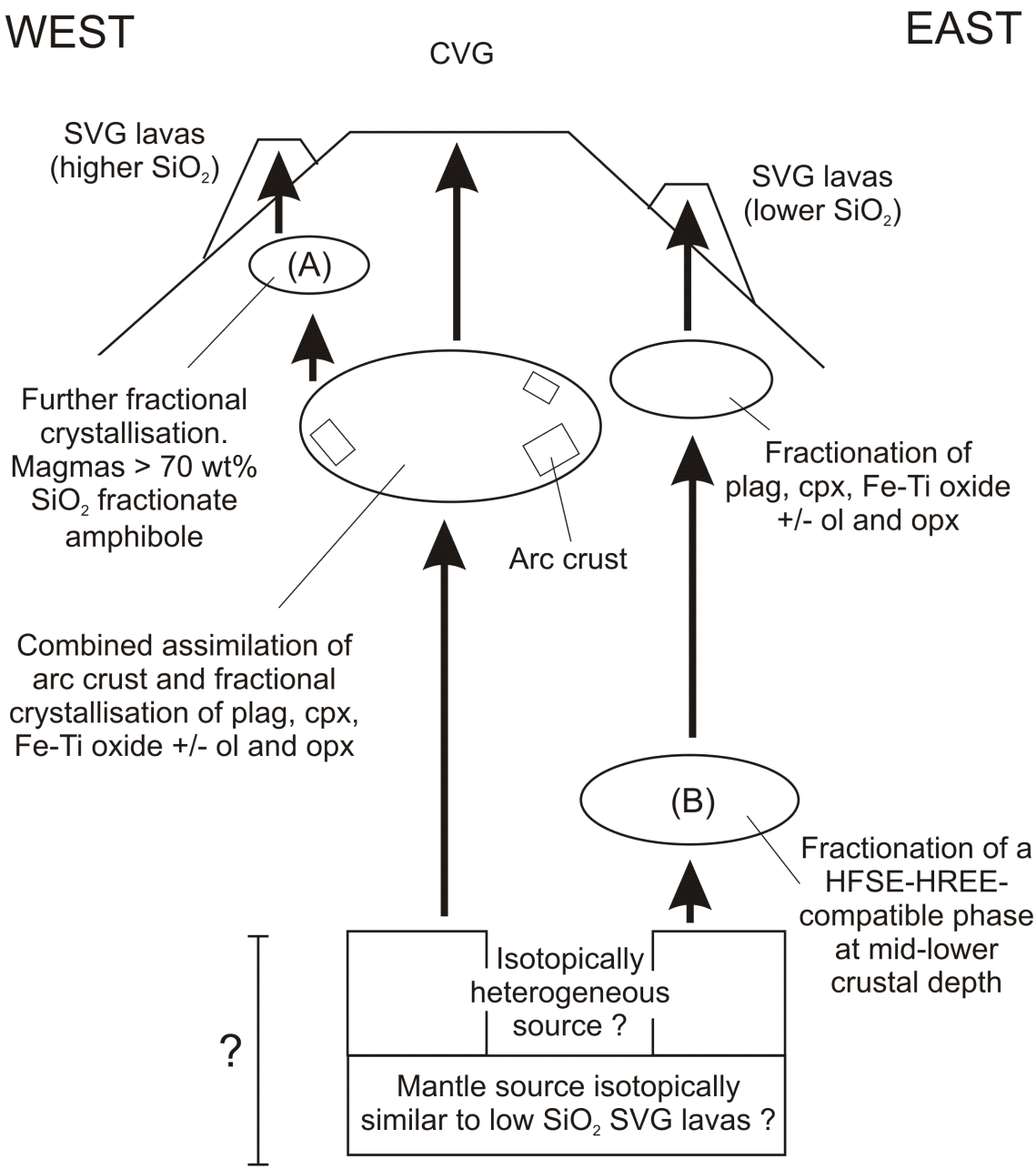
WEST
EAST
CVG
SVG lavas (higher $SiO_2$)
SVG lavas (lower $SiO_2$)
(A)
Further fractional crystallisation. Magmas > 70 wt% $SiO_2$ fractionate amphibole
Arc crust
Fractionation of plag, cpx, Fe-Ti oxide +/- ol and opx
Combined assimilation of arc crust and fractional crystallisation of plag, cpx, Fe-Ti oxide +/- ol and opx
(B)
Fractionation of a HFSE-HREE-compatible phase at mid-lower crustal depth
Isotopically heterogeneous source ?
Mantle source isotopically similar to low $SiO_2$ SVG lavas ?
?

**Table 1**
**Click here to download Table: Table_1.xls**

Table 1
Modal proportions of mineral phases in selected Salak volcanic rocks

| | CVG | | | | | | | | |
|---|---|---|---|---|---|---|---|---|---|
| | S104 | S105 | S106A | S106B | S108 | S109 | S110A | S110B | S111 |
| Ol | 2.1 | 4.2 | 3.3 | 3.2 | - | 1.9 | - | - | 9.1 |
| Opx | 1 | 0.8 | 7.2 | 5.9 | 2.3 | 3.2 | 4.2 | 3.2 | - |
| Cpx | 0.3 | 0.4 | 2.1 | 3.8 | 1.4 | 7.1 | 4.3 | 2.1 | - |
| Plag | 26.4 | 32.8 | 31.2 | 32.3 | 15.5 | 28.6 | 14.3 | 12.7 | 31.5 |
| Ox | 1.1 | 1.8 | 2 | 2 | 1.9 | 2 | 2.1 | 1.5 | 2.1 |
| Hbl | - | - | - | - | - | - | - | - | - |
| Bio | - | - | - | - | - | - | - | - | - |
| Qtz | - | - | - | - | - | - | - | - | - |
| GM | 69.1 | 60 | 54.2 | 52.8 | 78.9 | 57.2 | 75.1 | 80.5 | 57.3 |

| | SVG | | | | SL3 | Pre-Salak |
|---|---|---|---|---|---|---|
| | S102 | S103 | S107B | S102XEN | S112 | S101 |
| Ol | - | - | - | - | - | - |
| Opx | 6.2 | 10.8 | - | 2.7 | 7.4 | 1.5 |
| Cpx | 5.1 | 9 | 0.1 | 4.6 | 10.2 | 0.25 |
| Plag | 34.3 | 35.4 | 4.3 | 10.3 | 41.1 | 8.2 |
| Ox | 2.9 | 3.9 | 0.5 | 1.7 | 4 | - |
| Hbl | - | - | 0.25 | - | - | 0.25 |
| Bio | - | - | 0.25 | - | - | - |
| Qtz | - | - | 1.5 | - | - | 0.5 |
| GM | 51.5 | 40.9 | 93.1 | 80.7 | 37.3 | 89.3 |

Modal phase volume (%) established from point-counting between 200-300 points per sample. Ol, olivine; Opx, orthopyroxene; Cpx, clinopyroxene; Plag, plagioclase; Ox, Fe-Ti oxide; Hbl, hornblende; Bio, biotite; Qtz, quartz; GM, groundmass; XEN, xenolith.

**Table 2**

**Click here to download Table: Table_2new.xls**

Table 2

Representative chemical analyses of olivines

| Group | CVG | | | |
|---|---|---|---|---|
| Sample | S106B | S106B | S111 | S111 |
| Grain-Position | INC | P2-M | P2 | P3 |
| $SiO_2$ | 36.27 | 35.09 | 35.14 | 36.42 |
| $TiO_2$ | 0.01 | 0.02 | 0.05 | 0.04 |
| $Cr_2O_3$ | 0.00 | 0.00 | 0.00 | 0.01 |
| MgO | 32.79 | 27.32 | 25.64 | 29.66 |
| CaO | 0.17 | 0.19 | 0.22 | 0.18 |
| MnO | 0.58 | 0.82 | 0.82 | 0.71 |
| FeO | 29.60 | 36.65 | 38.66 | 33.94 |
| NiO | 0.01 | 0.01 | 0.04 | 0.03 |
| $Na_2O$ | 0.01 | 0.01 | 0.00 | 0.00 |
| Total | 99.44 | 100.10 | 100.56 | 100.99 |
| Si | 0.99 | 0.99 | 0.99 | 1.00 |
| Fe(ii) | 0.67 | 0.86 | 0.91 | 0.78 |
| Mn | 0.01 | 0.02 | 0.02 | 0.02 |
| Mg | 1.33 | 1.14 | 1.08 | 1.21 |
| Ca | 0.00 | 0.01 | 0.01 | 0.01 |
| Total | 3.02 | 3.02 | 3.01 | 3.01 |
| Fo | 66.39 | 57.06 | 54.18 | 60.91 |
| Fa | 33.61 | 42.94 | 45.82 | 39.09 |

Grain: P#, phenocryst; INC, inclusion.
Position: M, mid point.
Fo, forsterite content; Fa, fayalite content.
Structural formula based on 4 oxygens.

**Table 3**

**Click here to download Table: Table_3new.xls**

Table 3

Representative mineral chemical analyses of pyroxenes

| Clinopyroxene | | | | | | Orthopyroxene | | | | | |
|---|---|---|---|---|---|---|---|---|---|---|---|
| Group | CVG | | SVG | | SL3 | CVG | | SVG | | | SL3 |
| Sample | S106B | S110B | S102 | S102(XEN) | S112 | S106B | S110B | S102 | S102(XEN) | S102(XEN) | S112 |
| Grain-Position | P1-R | P1 | P1*R | P2 | P1-M | P1-R | P1 | P1-C | P1 | P3 | P2-C |
| $SiO_2$ | 49.92 | 50.64 | 51.24 | 52.78 | 50.99 | 52.71 | 51.93 | 51.68 | 51.88 | 53.37 | 52.25 |
| $TiO_2$ | 0.68 | 0.70 | 0.37 | 0.49 | 0.26 | 0.32 | 0.40 | 0.21 | 0.19 | 0.22 | 0.23 |
| $Al_2O_3$ | 3.42 | 2.21 | 1.47 | 1.83 | 1.07 | 2.09 | 1.20 | 1.00 | 1.23 | 0.65 | 0.88 |
| $Cr_2O_3$ | 0.00 | 0.00 | 0.01 | 0.00 | 0.00 | 0.00 | 0.01 | 0.00 | 0.02 | 0.02 | 0.01 |
| $Fe_2O_3$ | 4.23 | 3.65 | 3.70 | 0.79 | 3.97 | 1.73 | 1.81 | 2.67 | 2.18 | 1.37 | 2.26 |
| FeO | 6.79 | 9.05 | 7.36 | 9.63 | 7.85 | 16.50 | 20.13 | 21.43 | 20.81 | 17.88 | 20.91 |
| MnO | 0.35 | 0.47 | 0.50 | 0.48 | 0.51 | 0.48 | 0.68 | 1.02 | 0.92 | 0.63 | 0.70 |
| MgO | 15.10 | 14.33 | 15.54 | 15.15 | 13.70 | 24.80 | 21.97 | 21.00 | 21.54 | 24.24 | 21.76 |
| CaO | 19.28 | 19.26 | 19.48 | 19.64 | 21.13 | 1.63 | 1.83 | 1.46 | 1.49 | 1.69 | 1.67 |
| $Na_2O$ | 0.33 | 0.31 | 0.23 | 0.27 | 0.29 | 0.01 | 0.03 | 0.04 | 0.03 | 0.03 | 0.03 |
| $K_2O$ | 0.00 | 0.00 | 0.00 | 0.01 | 0.00 | 0.00 | 0.00 | 0.01 | 0.00 | 0.00 | 0.00 |
| NiO | 0.01 | 0.01 | 0.01 | 0.00 | 0.01 | 0.00 | 0.00 | 0.01 | 0.00 | 0.00 | 0.00 |
| Total | 100.11 | 100.61 | 99.91 | 101.07 | 99.78 | 100.27 | 99.99 | 100.52 | 100.30 | 100.09 | 100.70 |
| Si | 1.88 | 1.91 | 1.93 | 1.95 | 1.94 | 1.93 | 1.95 | 1.95 | 1.95 | 1.97 | 1.95 |
| Al | 0.15 | 0.10 | 0.07 | 0.08 | 0.05 | 0.09 | 0.05 | 0.04 | 0.05 | 0.03 | 0.04 |
| Fe(ii) | 0.21 | 0.28 | 0.23 | 0.30 | 0.25 | 0.50 | 0.63 | 0.67 | 0.65 | 0.55 | 0.65 |
| Fe(iii) | 0.12 | 0.10 | 0.10 | 0.02 | 0.11 | 0.05 | 0.05 | 0.08 | 0.06 | 0.04 | 0.06 |
| Cr | 0.00 | 0.00 | 0.00 | 0.00 | 0.00 | 0.00 | 0.00 | 0.00 | 0.00 | 0.00 | 0.00 |
| Ti | 0.02 | 0.02 | 0.01 | 0.01 | 0.01 | 0.01 | 0.01 | 0.01 | 0.01 | 0.01 | 0.01 |
| Mn | 0.01 | 0.02 | 0.02 | 0.02 | 0.02 | 0.01 | 0.02 | 0.03 | 0.03 | 0.02 | 0.02 |
| Mg | 0.85 | 0.80 | 0.87 | 0.83 | 0.78 | 1.35 | 1.23 | 1.18 | 1.21 | 1.33 | 1.21 |
| Ca | 0.78 | 0.78 | 0.79 | 0.78 | 0.86 | 0.06 | 0.07 | 0.06 | 0.06 | 0.07 | 0.07 |
| Na | 0.02 | 0.02 | 0.02 | 0.02 | 0.02 | 0.00 | 0.00 | 0.00 | 0.00 | 0.00 | 0.00 |
| Total | 4.04 | 4.03 | 4.03 | 4.01 | 4.03 | 4.01 | 4.01 | 4.02 | 4.02 | 4.01 | 4.02 |
| Wo | 39.54 | 39.21 | 39.15 | 39.94 | 42.75 | 3.22 | 3.68 | 2.92 | 2.99 | 3.33 | 3.31 |
| En | 43.10 | 40.59 | 43.45 | 42.89 | 38.58 | 68.25 | 61.33 | 58.48 | 60.10 | 66.41 | 60.18 |
| Fs | 17.36 | 20.20 | 17.40 | 17.17 | 18.67 | 28.53 | 35.00 | 38.60 | 36.91 | 30.26 | 36.51 |

Grain: P#, phenocryst; *mantling orthopyroxene. XEN = xenolith. Position: C, core; M, mid point; R, rim.
Wo, wollastonite content; En, enstatite content; Fs, ferrosilite content. Structral formula based on 6 oxygens.
Fe(iii) = 2X(1-T/S), where X = number of oxygens, T and S = correct and observed cation totals, respectively.

**Table 4**

**Click here to download Table: Table_4new.xls**

Table 4

Representative mineral chemical analyses of plagioclase

| Group | CVG | | | | | SVG | | | | SL3 | |
|---|---|---|---|---|---|---|---|---|---|---|---|
| Sample | S106B | S106B | S110B | S111 | S111 | S102 | S102 | S102(XEN) | S102(XEN) | S112 | S112 |
| Grain-Position | P3-M | P4-R | P3-C | GM | P4-R | P2-C | P2-R | P2-C | P2-M | P3-C | P3-R |
| $SiO_2$ | 45.33 | 51.16 | 53.97 | 55.44 | 45.66 | 54.69 | 53.72 | 53.87 | 48.00 | 54.10 | 52.46 |
| $TiO_2$ | 0.01 | 0.04 | 0.05 | 0.07 | 0.01 | 0.04 | 0.02 | 0.02 | 0.03 | 0.02 | 0.03 |
| $Al_2O_3$ | 33.88 | 29.59 | 28.19 | 27.05 | 34.05 | 27.57 | 27.77 | 28.05 | 31.69 | 27.71 | 28.94 |
| MgO | 0.05 | 0.08 | 0.07 | 0.06 | 0.02 | 0.05 | 0.05 | 0.04 | 0.07 | 0.05 | 0.05 |
| CaO | 18.56 | 13.85 | 11.90 | 11.04 | 18.60 | 11.09 | 11.45 | 11.83 | 16.37 | 11.45 | 13.03 |
| MnO | 0.02 | 0.00 | 0.02 | 0.00 | 0.00 | 0.01 | 0.00 | 0.00 | 0.00 | 0.00 | 0.02 |
| FeO | 0.60 | 0.66 | 0.59 | 1.22 | 0.62 | 0.41 | 0.57 | 0.48 | 0.51 | 0.45 | 0.54 |
| $Na_2O$ | 1.16 | 3.80 | 4.97 | 5.50 | 1.08 | 5.42 | 5.26 | 4.94 | 2.41 | 5.27 | 4.42 |
| $K_2O$ | 0.03 | 0.11 | 0.21 | 0.31 | 0.02 | 0.14 | 0.13 | 0.11 | 0.02 | 0.22 | 0.17 |
| Total | 99.63 | 99.29 | 99.96 | 100.69 | 100.05 | 99.41 | 98.95 | 99.34 | 99.09 | 99.27 | 99.64 |
| Si | 8.43 | 9.41 | 9.81 | 10.01 | 8.44 | 9.96 | 9.85 | 9.83 | 8.91 | 9.88 | 9.59 |
| Al | 7.42 | 6.42 | 6.04 | 5.76 | 7.42 | 5.92 | 6.00 | 6.03 | 6.93 | 5.97 | 6.24 |
| Fe | 0.09 | 0.10 | 0.09 | 0.18 | 0.10 | 0.06 | 0.09 | 0.07 | 0.08 | 0.07 | 0.08 |
| Ca | 3.70 | 2.73 | 2.32 | 2.14 | 3.68 | 2.16 | 2.25 | 2.31 | 3.25 | 2.24 | 2.55 |
| Na | 0.42 | 1.36 | 1.75 | 1.93 | 0.39 | 1.91 | 1.87 | 1.75 | 0.87 | 1.87 | 1.57 |
| K | 0.01 | 0.03 | 0.05 | 0.07 | 0.00 | 0.03 | 0.03 | 0.03 | 0.00 | 0.05 | 0.04 |
| Mg | 0.01 | 0.02 | 0.02 | 0.02 | 0.00 | 0.01 | 0.01 | 0.01 | 0.02 | 0.01 | 0.01 |
| Total | 20.07 | 20.06 | 20.07 | 20.10 | 20.04 | 20.05 | 20.10 | 20.04 | 20.06 | 20.09 | 20.09 |
| An | 89.72 | 66.38 | 56.30 | 51.69 | 90.45 | 52.64 | 54.20 | 56.59 | 78.92 | 53.87 | 61.39 |
| Ab | 10.13 | 32.98 | 42.51 | 46.61 | 9.46 | 46.60 | 45.06 | 42.77 | 20.98 | 44.89 | 37.68 |
| Or | 0.15 | 0.63 | 1.19 | 1.71 | 0.09 | 0.76 | 0.74 | 0.64 | 0.10 | 1.24 | 0.93 |

Grain: P#, phenocryst; GM, groundmass. Position: C, core; M, mid point; R, rim. Structural formula based on 32 oxygens.
XEN, xenolith within rock. An, anorthite content; Ab, albite content; Or, orthoclase content.

**Table 5**

**Click here to download Table: Table_5new.xls**

Table 5

Representative mineral chemical analyses of Fe-Ti oxides

| Group | CVG | | | | | | | | | SVG | | | | SL3 | | | | |
|---|---|---|---|---|---|---|---|---|---|---|---|---|---|---|---|---|---|---|
| Sample | S106B | S106B | S106B | S110B | S110B | S110B | S111 | S111 | S111 | S102 | S102 | S102(XEN) | S102(XEN) | S112 | S112 | S112 | S112 | S112 |
| Grain-Position | P1-C | P2-C | P3 | INC | P1 | P2 | P1 | P2 | P3 | P1 | P2 | P1 | P2 | P1 | P2 | P3 | P4-C | P4-C |
| $SiO_2$ | 0.08 | 0.07 | 0.07 | 0.08 | 0.07 | 0.08 | 0.07 | 0.10 | 0.05 | 0.10 | 0.06 | 0.05 | 0.11 | 0.05 | 0.05 | 0.03 | 0.06 | 0.04 |
| $TiO_2$ | 11.05 | 11.32 | 15.56 | 15.95 | 18.18 | 15.03 | 10.29 | 12.77 | 11.18 | 11.64 | 12.85 | 9.68 | 46.52 | 13.32 | 13.78 | 13.52 | 13.45 | 13.46 |
| $Al_2O_3$ | 4.24 | 3.66 | 1.85 | 3.11 | 2.46 | 2.69 | 4.37 | 2.74 | 3.66 | 2.41 | 2.09 | 2.84 | 0.05 | 2.53 | 2.34 | 2.39 | 2.44 | 2.48 |
| $Cr_2O_3$ | 0.03 | 0.05 | 0.07 | 0.01 | 0.04 | 0.03 | 0.16 | 0.24 | 0.14 | 0.02 | 0.01 | 0.06 | 0.00 | 0.03 | 0.02 | 0.04 | 0.02 | 0.03 |
| $Fe_2O_3$ | 43.72 | 43.25 | 37.35 | 34.37 | 31.46 | 37.93 | 44.32 | 41.08 | 43.62 | 43.53 | 41.30 | 47.13 | 0.00 | 41.14 | 41.01 | 40.57 | 40.16 | 40.84 |
| FeO | 37.57 | 38.13 | 42.54 | 41.35 | 45.19 | 42.08 | 37.46 | 39.94 | 38.31 | 39.58 | 40.24 | 37.59 | 46.67 | 41.53 | 41.56 | 40.31 | 40.31 | 40.79 |
| MnO | 0.43 | 0.44 | 0.47 | 0.51 | 0.58 | 0.59 | 0.40 | 0.42 | 0.42 | 0.52 | 0.62 | 0.48 | 1.26 | 0.51 | 0.58 | 0.52 | 0.49 | 0.49 |
| MgO | 2.67 | 2.25 | 1.82 | 2.61 | 1.68 | 1.96 | 2.19 | 1.89 | 2.11 | 1.33 | 1.37 | 1.50 | 1.63 | 1.31 | 1.60 | 1.94 | 1.86 | 1.77 |
| CaO | 0.00 | 0.00 | 0.03 | 0.02 | 0.00 | 0.03 | 0.00 | 0.01 | 0.00 | 0.00 | 0.02 | 0.00 | 0.19 | 0.01 | 0.00 | 0.05 | 0.00 | 0.00 |
| Total | 99.79 | 99.15 | 99.75 | 98.00 | 99.66 | 100.42 | 99.26 | 99.19 | 99.48 | 99.12 | 98.55 | 99.32 | 96.42 | 100.42 | 100.93 | 99.37 | 98.79 | 99.90 |
| Si | 0.02 | 0.02 | 0.02 | 0.02 | 0.02 | 0.02 | 0.02 | 0.03 | 0.01 | 0.03 | 0.02 | 0.01 | 0.04 | 0.02 | 0.01 | 0.01 | 0.02 | 0.01 |
| Ti | 2.43 | 2.52 | 3.47 | 3.58 | 4.05 | 3.32 | 2.28 | 2.86 | 2.49 | 2.63 | 2.92 | 2.18 | 10.78 | 2.96 | 3.05 | 3.03 | 3.03 | 3.00 |
| Al | 1.46 | 1.28 | 0.65 | 1.09 | 0.86 | 0.93 | 1.52 | 0.96 | 1.27 | 0.85 | 0.74 | 1.00 | 0.02 | 0.88 | 0.81 | 0.84 | 0.86 | 0.87 |
| Cr | 0.01 | 0.01 | 0.02 | 0.00 | 0.01 | 0.01 | 0.04 | 0.06 | 0.03 | 0.00 | 0.00 | 0.01 | 0.00 | 0.01 | 0.01 | 0.01 | 0.00 | 0.01 |
| Fe(iii) | 9.62 | 9.63 | 8.35 | 7.71 | 7.00 | 8.38 | 9.84 | 9.20 | 9.70 | 9.83 | 9.38 | 10.61 | 0.00 | 9.16 | 9.07 | 9.08 | 9.04 | 9.10 |
| Fe(ii) | 9.19 | 9.44 | 10.56 | 10.31 | 11.18 | 10.33 | 9.24 | 9.94 | 9.46 | 9.93 | 10.16 | 9.40 | 12.03 | 10.27 | 10.21 | 10.03 | 10.09 | 10.11 |
| Mn | 0.11 | 0.11 | 0.12 | 0.13 | 0.14 | 0.15 | 0.10 | 0.11 | 0.10 | 0.13 | 0.16 | 0.12 | 0.33 | 0.13 | 0.14 | 0.13 | 0.12 | 0.12 |
| Mg | 1.16 | 0.99 | 0.81 | 1.16 | 0.74 | 0.86 | 0.96 | 0.84 | 0.93 | 0.59 | 0.62 | 0.67 | 0.75 | 0.58 | 0.70 | 0.86 | 0.83 | 0.78 |
| Ca | 0.00 | 0.00 | 0.01 | 0.01 | 0.00 | 0.01 | 0.00 | 0.00 | 0.00 | 0.00 | 0.01 | 0.00 | 0.06 | 0.00 | 0.00 | 0.01 | 0.00 | 0.00 |
| Total | 24.00 | 24.00 | 24.00 | 24.00 | 24.00 | 24.00 | 24.00 | 24.00 | 24.00 | 24.00 | 24.00 | 24.00 | 24.00 | 24.00 | 24.00 | 24.00 | 24.00 | 24.00 |
| $TiO_2$ | 11.97 | 12.21 | 16.30 | 17.40 | 19.17 | 15.82 | 11.17 | 13.61 | 12.01 | 12.29 | 13.62 | 10.25 | 49.92 | 13.88 | 14.30 | 14.32 | 14.32 | 14.15 |
| $Fe_2O_3$ | 47.35 | 46.66 | 39.14 | 37.50 | 33.17 | 39.90 | 48.14 | 43.80 | 46.85 | 45.94 | 43.75 | 49.93 | 0.00 | 42.86 | 42.56 | 42.98 | 42.76 | 42.95 |
| FeO | 40.69 | 41.13 | 44.57 | 45.11 | 47.65 | 44.28 | 40.69 | 42.58 | 41.14 | 41.77 | 42.63 | 39.82 | 50.08 | 43.26 | 43.14 | 42.70 | 42.92 | 42.90 |

Grain: P, phenocryst; GM, groundmass; GLOM, glomerocryst; INC, inclusion (mineral included within is stated in parentheses) XEN = xenolith.

Spot: C, core; M, mid point (number indicates relative position along transect from core to rim); R, rim. Structural formula based on 32 oxygens.

**Table 6**

**Click here to download Table: Table_6.xls**

Table 6

Whole rock major element, trace element and isotopic compositions of Salak volcanic rocks

| | CVG | | | | | | | | |
|---|---|---|---|---|---|---|---|---|---|
| Sample | S104 | S105 | S106A | S106B | S108 | S109 | S110A | S110B | S111 |
| $SiO_2$ | 54.90 | 54.09 | 54.01 | 53.77 | 57.50 | 56.58 | 59.97 | 60.57 | 53.66 |
| $Al_2O_3$ | 19.43 | 20.16 | 18.71 | 18.78 | 17.49 | 17.60 | 15.83 | 15.94 | 19.61 |
| $Fe_2O_3$ | 8.89 | 8.45 | 9.99 | 9.85 | 8.78 | 9.21 | 8.50 | 8.50 | 9.60 |
| MgO | 2.54 | 2.49 | 3.63 | 3.61 | 2.26 | 2.88 | 1.86 | 1.81 | 3.33 |
| CaO | 7.70 | 8.79 | 8.38 | 8.39 | 6.20 | 6.89 | 5.14 | 4.98 | 8.67 |
| $Na_2O$ | 3.60 | 3.56 | 3.35 | 3.48 | 4.15 | 3.85 | 4.26 | 4.29 | 3.32 |
| $K_2O$ | 1.03 | 0.93 | 0.83 | 0.84 | 1.56 | 1.34 | 2.07 | 2.11 | 0.80 |
| $TiO_2$ | 1.04 | 0.97 | 1.02 | 1.01 | 1.15 | 1.18 | 1.16 | 1.17 | 0.98 |
| MnO | 0.17 | 0.17 | 0.19 | 0.19 | 0.21 | 0.20 | 0.19 | 0.16 | 0.18 |
| $P_2O_5$ | 0.33 | 0.26 | 0.26 | 0.26 | 0.40 | 0.28 | 0.48 | 0.48 | 0.28 |
| LOI | 0.48 | -0.13 | -0.05 | 0.05 | 0.16 | 0.01 | 0.08 | 0.15 | -0.08 |
| Total | 100.12 | 99.74 | 100.32 | 100.22 | 99.86 | 100.01 | 99.54 | 100.17 | 100.36 |
| | | | | | | | | | |
| Sc | 23 | 20 | 23 | 23 | 24 | 27 | 24 | 23 | 20 |
| Ti | 6851 | 6683 | 6671 | 6605 | 7618 | 7876 | 7750 | 7726 | 5568 |
| V | 160 | 143 | 178 | 177 | 99 | 161 | 75 | 74 | 164 |
| Cr | 2.2 | 1.1 | 2.4 | 4.3 | 0.4 | 0.5 | 0.3 | 0.9 | 7.7 |
| Mn | 1262 | 1239 | 1727 | 1743 | 1928 | 1835 | 1750 | 1193 | 1495 |
| Co | 19 | 18 | 22 | 22 | 14 | 17 | 13 | 10 | 21 |
| Ni | 4.7 | 1.5 | 4.3 | 4.2 | 0.8 | 1.1 | 1.1 | 0.9 | 8.1 |
| Cu | 52 | 26 | 38 | 36 | 38 | 35 | 54 | 41 | 18 |
| Zn | 72 | 58 | 70 | 74 | 87 | 73 | 81 | 76 | 70 |
| Ga | 20 | 19 | 19 | 19 | 19 | 19 | 19 | 19 | 19 |
| Rb | 33.8 | 27.8 | 23.7 | 23.8 | 52.3 | 44.4 | 68.8 | 74.1 | 22.4 |
| Sr | 374 | 451 | 422 | 422 | 354 | 358 | 292 | 291 | 395 |
| Y | 41 | 35 | 32 | 37 | 55 | 52 | 67 | 69 | 33 |
| Zr | 188 | 140 | 125 | 125 | 226 | 189 | 311 | 310 | 133 |
| Nb | 8.15 | 6.04 | 5.25 | 5.21 | 9.99 | 7.87 | 13.67 | 13.76 | 5.65 |
| Cs | 2.27 | 0.99 | 0.75 | 0.95 | 2.80 | 2.31 | 3.83 | 4.13 | 0.78 |
| Ba | 214 | 194 | 173 | 176 | 304 | 253 | 368 | 366 | 188 |
| | | | | | | | | | |
| La | 18.1 | 13.7 | 12.9 | 16.2 | 22.5 | 19.2 | 29.3 | 30.1 | 14.0 |
| Ce | 41.6 | 31.9 | 29.2 | 29.8 | 52.1 | 41.7 | 68.2 | 65.9 | 32.4 |
| Pr | 6.07 | 4.68 | 4.32 | 5.20 | 7.56 | 6.29 | 9.76 | 10.09 | 4.79 |
| Nd | 27.6 | 21.6 | 20.0 | 24.2 | 34.5 | 28.7 | 44.2 | 45.3 | 22.2 |
| Sm | 6.48 | 5.20 | 4.84 | 5.67 | 8.33 | 6.95 | 10.43 | 10.65 | 5.28 |
| Eu | 1.86 | 1.54 | 1.44 | 1.68 | 2.06 | 1.82 | 2.33 | 2.35 | 1.58 |
| Gd | 6.79 | 5.70 | 5.25 | 6.19 | 8.93 | 7.50 | 11.03 | 11.24 | 5.68 |
| Tb | 1.08 | 0.91 | 0.83 | 0.98 | 1.45 | 1.24 | 1.77 | 1.83 | 0.90 |
| Dy | 6.52 | 5.50 | 4.96 | 5.83 | 8.69 | 7.55 | 10.67 | 10.99 | 5.33 |
| Ho | 1.36 | 1.17 | 1.05 | 1.22 | 1.83 | 1.63 | 2.25 | 2.35 | 1.13 |
| Er | 3.77 | 3.24 | 2.90 | 3.36 | 5.06 | 4.56 | 6.27 | 6.42 | 3.09 |
| Tm | 0.60 | 0.51 | 0.46 | 0.51 | 0.79 | 0.71 | 0.97 | 1.02 | 0.48 |
| Yb | 3.84 | 3.28 | 2.94 | 3.29 | 5.08 | 4.57 | 6.31 | 6.54 | 3.07 |
| Lu | 0.64 | 0.54 | 0.49 | 0.55 | 0.85 | 0.77 | 1.07 | 1.08 | 0.52 |
| | | | | | | | | | |
| Hf | 4.58 | 3.58 | 3.23 | 3.19 | 5.82 | 4.87 | 7.94 | 7.93 | 3.41 |
| Ta | 0.47 | 0.34 | 0.30 | 0.31 | 0.60 | 0.47 | 0.81 | 0.87 | 0.33 |
| Pb (total) | 7.0 | 6.3 | 4.7 | 6.8 | 13.8 | 9.2 | 16.1 | 22.6 | 5.3 |
| Th | 3.49 | 2.87 | 2.44 | 2.43 | 5.94 | 4.66 | 7.88 | 7.90 | 2.51 |
| U | 0.81 | 0.64 | 0.56 | 0.56 | 1.32 | 1.02 | 1.72 | 1.74 | 0.58 |
| $^{87}Sr/^{86}Sr_m$ | | | 0.704671±9 | 0.704639±9 | | 0.704745±9 | 0.704778±10 | | 0.704596±10 |
| $^{143}Nd/^{144}Nd_m$ | | | 0.512735±7 | 0.512738±6 | | 0.512741±6 | 0.512723±8 | | 0.512746±9 |
| $^{176}Hf/^{177}Hf_m$ | | | 0.283055±9 | 0.283040±6 | | 0.283050±6 | 0.283041±6 | | 0.283046±28 |

Major element contents in wt%; trace elements concentrations in ppm; $_m$ = measured; isotope ratios ± 2SE (2*standard internal error).

**Table 7**
**Click here to download Table: Table_7.xls**

Table 7
Oxygen isotope data ($\delta^{18}O$) of mineral separates from Salak volcanic rocks

| | clinopyroxene | plagioclase |
|---|---|---|
| S100 | | 6.03 |
| S103 | 5.18 | 5.97 |
| S106A | 5.37 | |
| S111 | | 5.96 |
| S112 | 5.44 | 6.07 |

Table 8
End member compositions used in modelling calculations

| | Sample | Type | Element Concentrations (ppm) K | Rb | Ba | Th | Yb |
|---|---|---|---|---|---|---|---|
| | S106B | Salak basaltic andesite | 3470 | 24 | 176 | 2.4 | 3.29 |
| A | 107A | Salak rhyolite | 16545 | 158 | 582 | 20.1 | 2.24 |
| B | 75415 | Sumatran granitoid | 14652 | 237 | 12 | 34.9 | 1.35 |
| C | GU1/T | Javan tholeiite | 1374 | 3.4 | 97 | 0.8 | 2.94 |
| D | 75413 | Sumatran granitoid | 17101 | 68 | 937 | 5.9 | 1.86 |

Sumatran granitoid data from Gasparon (1993); Javan tholeiite from Guntur (Edwards, 1990); Salak samples from this study

**Table 9**
**Click here to download Table: Table_9new.xls**

Table 9

Summary of least squares major element modelling calculations for CVG rocks

| Model | | 1 | 2 | 3 | 4 |
|---|---|---|---|---|---|
| Parent | | S106B | S106B | S106B | S106B |
| Daughter | | S110B | S108 | S104 | S104 |
| $SiO_2$ range (%) | | 53.8-60.6 | 53.8-57.5 | 53.8-54.9 | 53.8-54.9 |
| $\Sigma r^2$ | | 0.13 | 0.13 | 0.01 | 0.01 |
| % of phase | Plag | 43.4 | 32.9 | 10.6 | 8.2 |
| removed | Cpx | 6.0 | 5.7 | 4.3 | 4.5 |
| relative | Ol | - | - | - | 2.7 |
| to initial | Opx | 7.9 | 6.1 | 3.5 | - |
| magma | Ox | 3.9 | 3.0 | 1.6 | 0.8 |
| %C | | 61 | 48 | 20 | 16 |

%C = percentage of crystallisation (sum of phases removed)
The mineral phases considered in modelling are limited to those observed as phenocrysts in either the parent or daughter rocks.

**Table 10**
**Click here to download Table: Table_10new.xls**

Table 10
Results of trace element Rayleigh Fractionation modelling

| Element | Yb | Ti | Y |
|---|---|---|---|
| normalised phase proportions | | | |
| Plag | 70.97 | 70.97 | 70.97 |
| Opx | 12.84 | 12.84 | 12.84 |
| Cpx | 9.80 | 9.80 | 9.80 |
| Fe-Ti Ox | 6.40 | 6.40 | 6.40 |
| Parent concentration (Co) | 3.3 | 6605 | 37 |
| Degree of fractionation (F) | 0.39 | 0.39 | 0.39 |
| $D_{Plag}$ | 0.052 | 0.052 | 0.076 |
| $D_{Opx}$ | 0.283 | 0.423 | 0.028 |
| $D_{Cpx}$ | 0.661 | 0.350 | 0.860 |
| $D_{Fe\text{-}Ti\ Ox}$ | 0.218 | 9.500 | 0.322 |
| D (bulk) | 0.170 | 0.733 | 0.203 |
| Calculated daughter comp. (Cl) | **7.2** | **8500** | **79** |
| Measured daughter comp. (Cl) | **6.5** | **7726** | **69** |

Daughter (S110B) composition calculated by forward modelling of parent S106B using $Cl = Co.F^{(D-1)}$.
Phase proportions and degree of fractionation values used are those suggested by least squares modelling (Table 9, Model 1). Distribution coefficients (D) are average values for basaltic-dacitic systems from the GERM database (http://earthref.org/GERM/index.html).

**Table 11**
**Click here to download Table: Table_11new.xls**

Table 11

Trace element and $^{87}Sr/^{86}Sr$ isotope compositions of potential crustal contaminants

| | Sample no. | Rock Type | Sr (ppm) | $^{87}Sr/^{86}Sr$ | K/Rb | Ba/Th |
|---|---|---|---|---|---|---|
| 1 | VM33-75 | terrig.-bio. sediment | 196 | 0.70925 | 106 | 16 |
| 2 | VM33-79 | terrigenous mud | 160 | 0.70802 | 124 | 18 |
| 3 | CS | calcareous-organogenic sediment | 1258 | ~ 0.709 | 106 | 60 |
| 4 | 76100 | S-Type granite | 32 | 0.74036 | 185 | 0.2 |
| 5 | ME99AL16 | intrusive (51 wt % $SiO_2$) | 609 | 0.706155 | 118 | 77 |
| 6 | ME00AL42 | intrusive (62 wt % $SiO_2$) | 375 | 0.706600 | 126 | 53 |
| 7 | H110x | intrusive (51 wt % $SiO_2$) | 152 | 0.708561 | 139 | 292 |
| 8 | J82x | intrusive (hbl spessarite) | 173 | 0.705291 | 346 | 58 |
| 9 | GU1/T | Javan tholeiitic lava | 232 | 0.70393 | 404 | 127 |
| 10 | TAF43/6 | Tongan tholeiitic lava | 118 | 0.70388 | 519 | 344 |
| 11 | 417D-418A | altered oceanic crust | 118 | 0.704584 | 235 | 364 |
| 12 | M22 | basalt (ophiolitic) | 143 | - | 416[a] | 10 |
| 13 | P-15 | dolerite (ophiolitic) | 171 | - | 4150 | 27 |
| 14 | S-134 | clinopyroxene gabbro (ophiolitic) | 129 | - | 1245 | 70 |

Data sources: 1-4: Gasparon 1993; Gasparon et al., 1998; 5-8: Elburg et al., 2005; 9: (Guntur tholeiite) Edwards, 1990; 10: Turner et al., 1997; 11: (average 417D-418A n = 7) Staudigel et al., 1996; 12-14 (Sulawesi ophiolite) Kadarusman et al., 2004.

[a] Rb concentration below detection limit therefore Rb abundance used is of sample P-33 (0.5 ppm) from the same area.